HE
18.5
.A38
NO.
DOT-
TSC-
142-1

T NO. DOT-TSC-142-1

Dept. Of Transportation
DEC 30 1974
Library

YSTEMATIC STUDY OF SUPERSONIC JET NOISE

JEAN F. LOUIS
DEPARTMENT OF AERONAUTICS AND ASTRONAUTICS
MASSACHUSETTS INSTITUTE OF TECHNOLOGY
CAMBRIDGE, MA. 02139

DECEMBER 1971
FINAL REPORT

transpo 72
U.S. International Transportation Exposition
Dulles International Airoort
Washington, D.C.
May 27-June 4, 1972

Availability is Unlimited. Document may be Released
To the National Technical Information Service,
Springfield, Virginia 22151, for Sale to the Public.

Prepared for:

DEPARTMENT OF TRANSPORTATION
TRANSPORTATION SYSTEMS CENTER
CAMBRIDGE, MA. 02142

The contents of this report reflect the views of Massachusetts Institute of Technology which is responsible for the facts and the accuracy of the data presented herein. The contents do not necessarily reflect the official views or policy of the Transportation Systems Center. This report does not constitute a standard, specification or regulation.

HE
18.5
.A38
no.
DOT-
TSC-
142-1

Dept. Of Transportation
DEC 20 1974
Library

TECHNICAL REPORT STANDARD TITLE PAGE

1. Report No.	2. Government Accession No.	3. Recipient's Catalog No.
DOT-TSC-142-1		

4. Title and Subtitle	5. Report Date
A Systematic Study of Supersonic Jet Noise	December 1971
	6. Performing Organization Code
7. Author(s)	8. Performing Organization Report No.
Jean F. Louis	
9. Performing Organization Name and Address	10. Work Unit No.
Department of Aeronautics and Astronautics Massachusetts Institute of Technology Cambridge, MA 02139	R-2519
	11. Contract or Grant No.
	DOT-TSC-142
12. Sponsoring Agency Name and Address	13. Type of Report and Period Covered
Office of Noise Abatement Department of Transportation Washington, D.C. 20590	Final Report
	14. Sponsoring Agency Code

15. Supplementary Notes

U.S. Dept. of Transportation, Transportation Systems Center.

16. Abstract

The purpose of this work is to study the acoustic fields associated with two different nozzle configurations; a rectangular and a circular. Both nozzles are designed with the same exit Mach number and have an identical momentum and energy flux..

The other main aim of this study is to establish scaling laws of supersonic jet noise. A shock tube is a very versatile apparatus for such an analysis. A short test time allows the use of a heat sink nozzle and eliminates the use of an anechoic chamber. So far tests have been made in the range of 1000-5000°R, for different levels of expansion and an exit Mach number of 2.7. In comparing the two nozzles, it is found that the rectangular nozzle is indeed quieter than the circular nozzle. The low acoustic efficiency of the over-expanded rectangular jet is related to a rapid deceleration of the jet through a system of strong shocks. At high temperature, this effect is not observed because an important density ratio exists across the shear layer which becomes very unstable due to the Taylor instability.

For both the circular and rectangular nozzle, the effect of temperature showed an increase in the directivity angle at high temperature which is correlated to an increase in eddy convective velocity, rather than refraction due to density gradients, which seems to play a secondary role.

The low temperature overexpanded jet showed a difference of about 2.6 db in the OPWL between the two nozzles. However, at this condition, for the rectangular nozzle, a difference of 8 db between the maximum and minimum noise direction is observed.

17. Key Words	18. Distribution Statement
Supersonic Jet noise Axisymmetric nozzle Turbulent mixing Rectangular nozzle Shock unsteadiness Mach wave Turbulence shock interaction	Availability is Unlimited. Document may be Released To the National Technical Information Service, Springfield, Virginia 22151, for Sale to the Public.

19. Security Classif. (of this report)	20. Security Classif. (of this page)	21. No. of Pages	22. Price
unclassified	unclassified	64	

Form DOT F 1700.7 (8-69)

PREFACE

The work on a systematic study of supersonic jet noise using a shock tunnel was first started under NASA Grant NGL 22-009-383 and Mr. James P. Kornberg carried out early experiments on the rectangular nozzle.

More recently, Messrs. Richard P. Letty and Jayanti R. Patel contributed to the measurements and analyses of supersonic jet noise sponsored under DOT Contract TSC-142.

This technical report was monitored by Mr. Raymond Ehrenbeck, DOT Transportation Systems Center.

TABLE OF CONTENTS

I.	INTRODUCTION AND SURVEY	1
	1.1 Mach Waves	1
	1.2 Shock Turbulence Interaction and Shock Unsteadiness	1
	1.3 Nozzle Lip Radiation	1
	1.4 Turbulent Mixing	2
II.	EXPERIMENTAL APPARATUS AND TECHNIQUE	7
	2.1 Equipment	7
	2.2 Data Acquisition	10
	2.3 Data Reduction	12
III.	RESULTS AND DISCUSSION	15
	3.1 Low Temperature Analysis (1350°R)	15
	3.2 Directivity Pattern	15
	3.3 Ellipticity	17
	3.4 Frequency Spectra	17
	3.5 Sound Power Level	18
	3.6 Shadowgraphs	21
IV.	HIGH TEMPERATURE ANALYSIS (4900°R)	25
	4.1 Directivity Patterns	25
	4.2 Ellipticity	27
	4.3 Shadowgraphs	28
	4.4 Acoustic Efficiency and Total Power Level	29
V.	INTERMEDIATE TEMPERATURE ANALYSIS (2900°R)	31
	5.1 Acoustic Efficiency and OPWL	31
	5.2 Scaling Laws	32
	5.3 Auto and Cross-correlation	36
VI.	CONCLUSIONS	38
REFERENCES		65

LIST OF FIGURES

Figure Number		Page Number
1	Time distance history in shock tunnel	41
2	Oscilloscope traces showing shock speed and test time, response of the B&K microphones	42
3	Circular and slotted (rectangular) nozzle	43
4	Schematic of data acquisition and reduction system	44
5	Digital signal; auto and cross correlation functions	45
6	Directivity pattern for perfectly expanded jet (low temperature) in the two nozzle axis: along long axis	46
7	Directivity pattern for perfectly expanded jet (low temperature) in the two nozzle axis: along short axis	46
8	Directivity patterns of the contours db levels for a stagnation temperature of 1350°R	47
9	Ellipticity as a function of axial distance on a cylindrical surface of radius 36" coaxial to jet	48
10	Characteristic frequency spectra along the long and the short axes	49
11	Frequency shift observed from the B&K microphone positions along the 144 db contour of the overexpanded jet (low temperature)	50
12	Frequency shift in a traverse direction to the jet axis (overexpanded rectangular jet)	51
13	Underexpanded rectangular jet shadowgraph along the long axis	52
14	Perfectly expanded jet shadowgraph along the short axis	53
15	Shadowgraph picture for the three expansion levels (rectangular jet)	54
16	Shadowgraph of the overexpanded low temperature (1350°R) circular jet	55

Figure Number		Page Number
17	Directivity pattern of the high stagnation temperature circular jet (4900°R)	56
18	Ellipticity as a function of axial distance on a cylindrical surface of radius 36" coaxial to jet (high temperature jet)	57
19	Axial distribution of intensity at discrete frequencies	58
20	High temperature (4900°R) perfectly expanded rectangular jet shadowgraph	59
21	Shadowgraph for high temperature (4900°R) overexpanded circular jet	60
22	Directivity patterns of the contours of constant db levels for a stagnation temperature of 2900°R (circular jet)	61
23	OPWL v/s 10 log $(\frac{p_o}{p_{o\ ref}})$ plot	62
24	Sound power level (PWL) of the perfectly expanded circular jet v/s stagnation temperature	63
25	Acoustic efficiency of the perfectly expanded (circular) jet v/s stagnation temperature	64

LIST OF SYMBOLS

A_e	exit area
C_o	speed of sound
D.F.T.	discrete Fourier transform
$F(\omega)$	Fourier transform of channel A
F.F.T.	fast Fourier transform
$G(\omega)$	Fourier transform of channel B
M_1	incident shock Mach number
M_e	nozzle exit Mach number
n	scaling factor
N	sampling point
OPWL	overall power level
PNdb	perceived noise level
PWL	sound power level
P_1	driven pressure
P_{o5}	stagnation pressure
P_n^2	mean SPL at a distance x from nozzle exit
SPL	sound pressure level
SPL_L	local sound pressure level
T_1	room temperature
T_{o5}	stagnation temperature
V_e	exit velocity
γ	specific heat ratio
ρ_a	ambient density
ρ_j	jet density at exit
$\eta_{acoustic}$	acoustic efficiency

Θ_M	Mach angle
Θ_S	directivity angle

ABSTRACT

A SYSTEMATIC STUDY OF SUPERSONIC JET NOISE

The purpose of this work is to study the acoustic fields associated with two different nozzle configurations; a rectangular and a circular. Both nozzles are designed with the same exit Mach number and have an identical momentum and energy flux. By presenting a comparison of the two nozzles, it it proposed to establish and identify the dominant noise generating mechanisms. A basic difference in shape changes the relative importance of different noise mechanisms.

The other main aim of this study is to establish scaling laws of supersonic jet noise. A shock tube is a very versatile apparatus for such an analysis. By first changing the driver, driven pressure and molecular weights, a wide range of stagnation pressures and temperatures could be achieved. The case with which these conditions are simulated is, however, traded off with the short test time, of the order of milliseconds. A short test time allows the use of a heat sink nozzle and eliminates the use of an anechoic chamber. So far tests have been made in the range of 1000-5000°R, for different levels of expansion and an exit Mach number of 2.7. In comparing the two nozzles, it is found that the rectangular nozzle is indeed quieter than the circular nozzle. The rectangular nozzle is more effective under overexpanded conditions, and a factor of 1.6 in acoustic efficiency at low temperature (1200°R) and about 3 at high temperature is related to a rapid deceleration of the jet through a system of strong shocks. The low acoustic efficiency of the overexpanded rectangular jet is related to a rapid deceleration of the jet through a system of strong shocks. At high temperature, this effect is not observed because an important density ratio exists across the shear layer which becomes very unstable due to the Taylor instability.

For both the circular and rectangular nozzle, the effect of temperature showed an increase in the directivity angle at high temperature which is correlated to an increase in eddy convective velocity, rather than refraction due to density gradients, which seems to play a secondary role.

The low temperature overexpanded jet showed a difference of about 2.6 db in the OPWL between the two nozzles. However, at this condition, for the rectangular nozzle, a difference of 8 db between the maximum and minimum noise direction is observed. Hence, a suitable orientation of the nozzle could cause a considerable reduction in the noise level. The rectangular nozzle seems to be very effective under overexpanded conditions.

The scaling laws, which are in the preliminary stages, were developed for the change in the OPWL as a function of stagnation pressure. For the circular nozzle, additional scaling was done for temperature and acoustic efficiency. These scaling laws need to be verified for additional temperatures. Also, further work should be initiated in the potential use of the rectangular nozzle as a noise suppressor and as a model for better comprehension of noise generating mechanisms.

CHAPTER I

INTRODUCTION AND SURVEY

Even after a period of about twenty years, when Lighthill[1] first published his theory on aerodynamic noise, the understanding of noise generating mechanisms is still quite controversial.[2,3,4,5] The subsonic jet noise, where no complex phenomenons as shock or eddy Mach noise exit, is based mainly on the turbulent mixing. The supersonic jet noise, on the other hand, is a cumulative effect of Mach wave radiation, nozzle lip radiation, shock turbulence interaction, shock unsteadiness and turbulent mixing.

1.1 Mach Waves

These are mainly due to disturbances convected supersonically, which radiate sound in a highly directional peak. They originate in a region of few jet diameters from the nozzle exit and their existence has been confirmed by shadowgraphs and recently by holographic techniques. Theoretical studies by Ffowcs Williams, Ribner and Phillips view these disturbances as eddies convecting within the shear layer, whereas others (Tam, Liu) consider these as instability waves propagating in the shear layer.

1.2 Shock Turbulence Interaction and Shock Unsteadiness

Their existence too is based on optical observations, which show spherical radiations centered at shock tips and propagating traverse to the jet axis. Their contribution to overall noise found so far is not substantial; nor is their influence with temperature credited. Turbulence interaction with shocks results in three different perturbation modes: vorticity, entropy and acoustic. It is this acoustic mode which propagates outwards.

1.3 Nozzle Lip Radiation

This noise radiation is associated with the turbulent flux coming out

of the nozzle and often convected on the turbulent layer. This radiation has a dipole characteristic at low speed but monopole at high speed.

1.4 Turbulent Mixing

Turbulent mixing which dominates subsonic jet noise is to some extent, with present theories, modelled as the main supersonic jet noise mechanism. According to these theories, the dominant aerodynamic noise location is centered in a region 20 diameters from nozzle exit, where transition (M=1) to subsonic flow takes place.

The exact contribution by each of the above to the total noise is not yet assessed. Mathematically, it becomes quite difficult to decouple them because of the complexity of their origin. It is only through experimental scaling laws that each mechanism could be analysed.

In dealing with noise suppression problems, any suppression would necessitate first a basic understanding of the noise generating mechanisms, and finding the sources which contribute the maximum. The dominating parameter is the jet velocity. The reason the noise problem has been difficult to solve is that the acoustic energy radiated is less than 1% of the jet KE, and a considerable change in KE has to be made before any appreciable change in acoustic energy results. However, in doing so, problems of reduced thrust and propulsive efficiency creep up. As such, the noise problem cannot be solved completely, but has to be optimized with aircraft performance.

In subsonic jets, the noise is reduced to a considerable extent with the use of bypass fans and corrugated lobe shaped nozzles which induce external air flow. Any noise reduction technique would involve:

1. Reducing the total sound power level (PWL).
2. Reducing the perceived noise level by shifting the power spectra to higher frequencies.
3. Redistributing the acoustic energy, which is creating a very directional acoustic pattern.

Early work on rectangular and multinozzle (subsonic) was abandoned with the development of less costly and more effective bypass turbofan engines. However, recently some work by Nagamatsu[8] came out on supersonic multinozzles. He predicted a reduction of about 22 db in PWL, but encountered a thrust loss of about 26%. In multinozzles, the factor controlling noise suppression is the area ratio and the number of tubes which indirectly result in rapid mixing of the jets, and hence reduce the mean velocity gradient.

Directional nozzles, especially the rectangular, besides reducing the PWL, are found to redistribute the acoustic energy in a plane traverse to the jet axis. In such cases, the noise distribution is found to be elliptical with maximum noise in a plane perpendicular to the long side.

The main purpose of this work is to study the acoustic fields associated with two different nozzle configurations; a rectangular and a circular. Both the nozzles are designed with the same exit Mach number and have an identical momentum and energy flux. A direct comparison of the results can be made since the testing conditions, the procedure for data acquisition, reduction and analysis are the same. By presenting a comparative study, we propose to establish and identify the dominant noise generating mechanisms. A basic difference in shape changes the relative importance of different noise generating mechanisms.

The other main aim of this study is to establish some scaling laws.

Mathematical analysis becomes complex due to many uncertainties involved and, as such, experimental scaling laws are to be developed. A shock tube is a very versatile apparatus for such analysis. By first changing the driver, driven pressures and molecular weights, a wide range of stagnation pressures and temperatures could be achieved. The ease with which these conditions are stimulated is, however, traded off with the short test time, of the order of milliseconds. A short test time has inherent advantages too.

1. No appreciable heating of the nozzle takes place, and therefore a heat sink nozzle can be used.
2. No anechoic chamber is required, and not much care regarding reverberation from walls is necessary.

The scaling laws are to be based on Mach numbers, stagnation temperature and pressure.

The ultimate aim of this work is noise abatement.

With these considerations, a rectangular and a circular nozzle of exit Mach number 2.7 were designed. The rectangular nozzle, with an exit aspect ratio of 6.78, is an initial design, with plans for modification to a multi-tube rectangular nozzle where use of the two main suppressor ideas (shielding and directivity) could be used. The effect of stagnation pressures over the SPL and acoustic efficiencies are to be investigated; this chiefly deals with the effect of shocks on noise production. The two nozzles are expected to exhibit different shock configurations and hence their interaction with shear layer is likely to be different.

Besides microphone analysis, shadowgraph pictures are to be taken and correlated with measured data. A word about shadowgraph technique is that it gives second derivative of density perturbation and weighs waves

according to their steepness and not their sound pressure level (SPL). Interferometry is an ideal way of studying these near field waves and source locations; this technique deals in direct density variation rather than first derivative of schlieren or second derivative of shadowgraphs. For high temperature jets the near field waves are overshadowed by the high level of turbulence, and this method would be ideal in such cases. Holographic technique could be used[13,14] to give a three dimensional flow field visualization which any other method cannot give.

CHAPTER II

EXPERIMENTAL APPARATUS AND TECHNIQUE

2.1 Equipment

When working at temperatures as high as 4900°R, it is necessary that the jet be stimulated as easily and as cheaply as possible. A shock tunnel serves as the easiest and fastest way of creating such hot jets. As mentioned earlier, the only limitation is in the test time, but this too can be overcome by fast signal processing. The next thing is to show the duration of the test time and the consistency of each run as regards the stagnation temperature and pressure. One method is to keep the incident shock speed constant, so that P_{o5} and T_{o5} are constant. A better method adopted was locating a microphone at some fixed distance from the jet-axis, and the SPL recorded. The variation in SPL from run to run gives the inconsistency of each run, which as found is quite negligible ($\pm$ 0.2 db).

The shock tunnel essentially consists of a high and a low pressure section separated by a thin diaphragm. As the diaphragm ruptures, a shock wave is created in the low pressure section and an expansion fan in the high pressure section. The incident shock, after reflecting from the partially opened end, leaves behind a region of high stagnation pressure and temperature. The duration for which this pressure and temperature remain constant is related to the test time. This duration is influenced by the relative lengths of driver and driven section, the gases used and their temperatures.

Figure 1 shows the shock tunnel operating principles; section 1 represents the test gas region and 4 the driver region. Regions 2 and 3 are separated by the interface, traveling at a slower speed compared to

shock speed. The rarefaction waves propagating upstream in region 4 are reflected by the end, and an expansion fan propagates downstream and in "tailored" condition. The test time duration is determined by this fan when it catches the interface. The reflected shock may bounce back as either a shock wave or a rarefaction wave, or just pass through the interface without changing the conditions on either side of it.[15]

When $a_2 > a_3$, the reflected shock, after passing through the interface, further increases its velocity and develops high pressure in region 8. In order to match the boundary conditions on either side of the interface, the pressure in region 7 has to increase and is achieved by a reflected shock from the interface. An expansion wave results when $a_2 < a_3$.

In order to increase the available test time, a "tailored-interface" technique is adopted. With properly controlled initial conditions in the driver and driven sections, the state of the gas behind the interface can be made such that the reflected shock passes through without changing its strength.

Tailoring condition is given by:

$$\frac{\gamma_2}{a_2^2}\left[(\gamma_2 + 1)\frac{p_2}{p_5} + \gamma_2 - 1\right] = \frac{\gamma_3}{a_3^2}\left[(\gamma_3 + 1)\frac{p_2}{p_5} + \gamma_3 - 1\right] \qquad (2\text{-}1)$$

$$\gamma_2 \neq \gamma_3$$

When $\gamma_2 = \gamma_3$ "tailoring" condition is $a_2 = a_3$.

However in doing this, one ends up with molecular weights in the driven section varying from 4 to 15, which necessitates the use of a mixture of gases, helium being the chief constituent with argon as the second fluid.

Argon and helium are chosen to have as high an initial sound speed

ratio $(\frac{a_4}{a_1})$ as possible.[16] This enables a stronger shock with low driver pressures.

The low temperature runs were carried out using air and argon and a good 15 msec. test time was obtained (Figure 2) without the need of "tailoring" the flow. The detailed calculations are not presented here; refer to reference 12.

On the shock tube are mounted three Kistler pressure transducers, connected to three miniature fixed gain feedback charge amplifiers and used for measuring the incident shock velocity. These transducers have a rise time of about 1 msec. and a normal sensitivity of 0.35 pcb/psi.

The driven gas pressure was accurately controlled, whereas a variation of 5 to 10% in the driver section pressure did not greatly affect the shock speed so as to change the stagnation pressure and temperature.

The relation for stagnation temperature and pressure is given by:

$$\frac{T_5}{T_1} = \frac{\{2(\gamma-1)M_1^2 + (3-\gamma)\}\{(3\gamma-1)M_1^2 - 2(\gamma-1)\}}{(\gamma+1)^2 M_1^2} \qquad (2\text{-}2)$$

$$\frac{P_5}{P_1} = \{\frac{2\gamma M_1^2 - (\gamma-1)}{\gamma+1}\}\{\frac{(3\gamma-1)M_1^2 - 2(\gamma-1)}{(\gamma+1)M_1^2 + 2}\}. \qquad (2\text{-}3)$$

The present work is associated with a rectangular and a circular nozzle (Figure 3) of identical Mach number of 2.7 and exit area of 0.154 in^2. Both these nozzles thus have identical momentum and energy flux. The rectangular nozzle was cast out of epoxy resin ERL 2256 combined with a hardener H-45 and fiberglass chips were added for strength and temperature resistance. The circular nozzle, which was computer designed, was cast out of aluminum. The rectangular nozzle, on the other hand, was designed in two parts; a convergent part which could be easily adapted to the shock

tube, and a divergent part which was designed to provide a source flow (radial flow in a disc shaped annulus). With this nozzle is associated a 3% drop in theoretical propulsive efficiency.[17]

With the help of 3 B&K 1/8" condenser microphones, the data is recorded on a 14 channel Ampex FR 1900 multiband instrument tape recorder. These microphones were particularly chosen for the high frequency range from 30 HZ to 140 KHZ and also have a high dynamic range up to 184 db. re. 0.0002 μ bars. These microphones need a regular calibration which is performed with a B&K 4220 piston phone which has a reference SPL of 124 db. at 250 HZ. On the tape recorder four FM channels are used, three for the microphones and one for a Kistler pressure transducer mounted at the exit of the nozzle; the signal from this channel is used to initiate the digital system. The frequency range of the tape recorder is from DC to 80 KHZ with signal to noise ratio of 53 db. The sampling frequency for the A/D convertor is supplied by a direct record channel, which is also the control track for the tape recorder and has an output of 200 KHZ supplied by a crystal oscillator. Because of the short duration of the test time, all recording is made at 120"/sec. and the playback is at 1 7/8"/sec.

2.2 Data Acquisition

For the rectangular nozzle, data was acquired at 1350°R and 4900°R, while for the circular nozzle, an intermediate temperature of 2900°R was also worked at. At each temperature, analysis is to be made at various expansion levels, basically to study the effect of different noise generating mechanisms.

For the circular nozzle, because of its axisymmetric nature, noise measurements are made in only one plane. However, for a rectangular nozzle,

to obtain a three-dimensional acoustic field, it is necessary to make measurements in three or four planes through the jet axis. The limitation to the number of microphones has restricted our survey in only two planes; in the plane of long axis and the short axis. Kornberg made measurements in the 45° plane.

The figure shown below indicates the nomenclature used in the subsequent text.

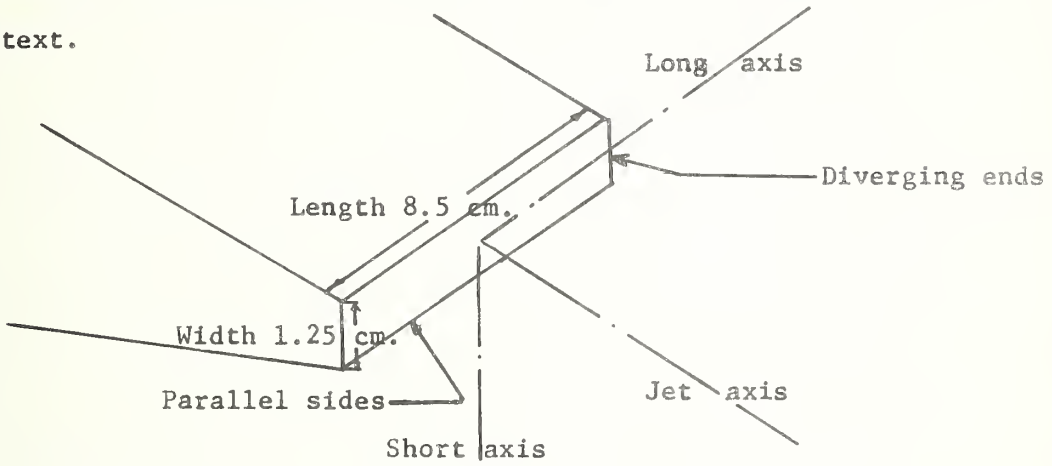

All the data acquisition is done at one Mach number (2.74). The microphones are always positioned traverse to the jet and the near and far field pressure fluctuations recorded; care being taken not to locate the microphones too close to the jet boundary. Through the cathode follower and the power supply, the data are transmitted on the tape. Even when recording at the fastest speed (120"/sec.), the length of the tape used for actual data is hardly an inch.

At the beginning of every set of runs, the microphones are calibrated and so are the tape recorder channels, which are checked for signal/noise ratio.

Typical oscilloscope pictures of the microphone recordings are shown in Figure 2. Also shown are the shock speed traces for both low and high temperatures. The high temperature traces, besides giving the shock speed, also indicate the duration of the test time.

2.3 Data Reduction

The limitation to the test time is a big trade-off with the ease and convenience of stimulating the necessary temperatures and pressures. This short test time limits the use of conventional methods used for analog signal analysis. Initially two methods were tried out with little success. One was to transfer the signal on to a continuous loop tape and feed the signal to a frequency analyser. The other method was to set the Ampex tape recorder on a rocking mode and then pass the signal to an analyser during each cycle. The signal during each cycle had to be gated, so as to eliminate extraneous noise, and also an initial 1 to 2 msec. data had to be eliminated, which corresponds to time required for flow to reach steady state.

The method which is presently used for data analysis is digital processing. A schematic is given in Figure 4 for the general reduction system. The signal is first reduced on an A/D convertor to binary values and is stored on a seven track digital tape. A subroutine converts these binary values into two one-dimensional arrays; voltage and time. The sampling frequency of 200 KHZ is reduced by a factor of 64 when the signal is played back at 1 7/8"/sec. In terms of real test time, the sampling interval is 5 msec. The digitised data is stored on tape in form of blocks, each block containing 1024 points. This number (2^8) is particularly suited when working with fast Fourier transforms, and using this value, the saving in computation time is up to 99% as compared to ordinary Fourier transforms.

When the data matrices are read on the computer, the input signal is plotted as a visual check on the A/D conversion process (Figure 5).

If f(nT) represents the sampled points, taking the Fourier transforms, the data is transformed from time to frequency domain.

$$F(\omega) = \sum_{n=o}^{1023} f(nT)\ e^{-j\omega nT} \qquad (2\text{-}4)$$

and similarly

$$G(\omega) = \sum_{n=o}^{1023} g(nT)\ e^{-j\omega nT}. \qquad (2\text{-}5)$$

Using the convolution property of Fourier transforms, which states that the integral of the function

$$[\ \int f(t)\ g(t - \tau)\ dt\ ] = F(\omega)\ \overline{G}(\omega) \qquad (2\text{-}6)$$

Function on left is nothing but the cross correlation of two signals f(t) and g(t) which is obtained by multiplying the Fourier transforms of the two signals, one of which is conjugate, and then taking the inverse Fourier transform. Auto-correlation becomes a particular case when f(t) = g(t). One way to find the spectral density is to take the Fourier transform of the so obtained auto-correlation. The auto and cross correlation are scaled for unity in each channel.

The output results are directly plotted on S.C. 4020 (Figure 5). The spectral density plots can be printed up to 100 KHZ, which is the Nyquist frequency. Actual plotting is done up to 50 KHZ, beyond which the magnitudes become small and the interested frequency range is from 1 to 25 KHZ.

A separate program calculates the RMS sound pressure level of each channel.

The main program at present has no provision for smoothing either the intensity spectrum plots or the auto and cross-correlation plots. It is felt, by increasing the sampling frequency from the present 200 KHZ to,

say, 600 KHZ, after analysing, an averaging process would give somewhat smoother curves.

CHAPTER III

RESULTS AND DISCUSSION

One of the objectives of this study is to establish the dominant noise generating mechanisms. By using two nozzles of different geometric configuration, the relative importance of noise generating mechanism changes. Also to be studied is the effect of jet stagnation temperature and pressure on the overall power level, which can then lead us to development of some scaling laws.

For the rectangular jet, the results are for two temperatures, a low temperature of around 1350°R, which is of the same order as a high speed jet engine exhaust, and the other at 4900°R, more related to rocket exhausts. For the circular nozzle, an intermediate temperature of 2900°R is also worked.

3.1 Low Temperature Analysis (1350°R)

For this temperature, the operating pressure ratios for the three expansion conditions are $(\frac{p_5}{p_o})$ 29/1, 23/1, 17/1; underexpanded, perfectly and overexpanded respectively. The nozzle, even when operated at perfect expansion conditions, exhibits some weak standing shocks.

3.2 Directivity Pattern

For each of the three pressure levels, directivity patterns are plotted. Because of the nonsymmetry of the rectangular nozzle, directivity patterns are plotted in two planes of the nozzle; along the long axis and along the short axis. Figures 6 and 7 represent the directivity pattern along the long and short axes for a perfectly expanded rectangular jet. Figure 8 compares the directivity pattern for the three conditions for the circular jet. From Figure 6 the peak directivity angle is observed to be

around 56° relative to the jet axis. The rectangular jet in the far field appears to be more directional along the long axis than the short. Also, as compared, the circular jet does not exhibit as big a directionality as along the long axis of rectangular jet.

Besides geometric effect, the directionality from the two sides of the rectangular nozzle may be due to:

1. Stronger Mach wave type radiation is observed along the longer side than the shorter.
2. More scattering along the long axis may induce a directional radiation pattern.
3. A difference in convective velocities of the eddies along the two sides of the jet.

In the circular nozzle, it is believed that supersonically convecting eddies give rise to the basic directivity pattern, which is modified by the refraction of sound sources by the jet temperature and hence density variation profile.

Operating at three different expansion levels, the eddy convective velocity is expected to vary, and so is the directivity field. However, for the rectangular nozzle, the far field directivity along the long axis does not vary much; a variation from 52° to 56° is observed.[23] The corresponding variation for the circular jet is between 44° and 53°. Shadowgraphs show the presence of strong shock system for the overexpanded circular jet, but this seems to have very little effect on the directivity. A question one may ask at this stage is whether it is the turbulent region or the Mach waves and lip radiation which dominates directivity. Although the exit density ratio $(\frac{\rho_j}{\rho_a})$ varies from 1.2 to 2.2 for the three expansion levels, it does not significantly affect the directivity.

3.3 Ellipticity

For the rectangular jet, there exist two directivity patterns along the two axes of the jet, and to this, we associate a function known as ellipticity. It is defined as the difference between the maximum and minimum SPL at different axial locations along the jet and on a cylindrical surface of radius R. Figure 9 shows the ellipticity of the traverse noise field for the three levels of expansion.

The results indicate a minimum of 3 db. ellipticity for this temperature (1350°R) over the axial length of the jet and a maximum in the region of maximum directivity.

3.4 Frequency Spectra

One of the reasons for studying the rectangular nozzles is noise suppression in the PN db. band. The dimensional characteristics of the rectangular nozzle to some extent exhibit a difference in the frequency distribution along the two axes of the nozzle. Figure 10 shows the difference in intensities at low and high frequencies; high frequencies are dominant along the short axis, being a function of the nozzle width. The circular nozzle exhibits somewhat intermediate levels at different frequencies. The spectra level would be to some extent influenced by the turbulent intensity and scales - which change as a function of distance from nozzle exit.

In order to show this frequency shift as a function of axial distance, intensity spectra are plotted on an isobar of 144 db. for an overexpanded circular jet (Figure 11). The off stream distance is 24". It indicates a shift from high to low frequencies towards the turbulent mixing region. For an overexpanded rectangular jet the intensity spectra is plotted as a function of off stream distance (Figure 12), which basically shows the attenua-

tion of high frequency noise with distance traverse to the jet. For this particular case, it was observed that the RMS SPL decreased from 152 db. to 139 db. in about 30". This is not surprising, for along the short axis high intensity at high frequencies is dominant.

3.5 Sound Power Level

Since the KE of the jet at nozzle exit for the three expansion levels is changing, a direct comparison of the local SPL cannot be made. Simcox[11], using different nozzles having different Mach numbers and with the same stagnation pressure, arrives at a normalizing parameter based on the mass flow rate:

$$SPL_c = SPL - 10 \log A_T \qquad A_T = \text{Throat area} \qquad (3\text{-}1)$$

$$SPL_c = \text{SPL corrected}$$

However, this is not the actual situation since mass flow rate would still affect the KE, and hence local pressure fluctuation. In his case, the data collapsed quite well.

The only way in which the noise level from a circular and rectangular jet could be compared is to calculate the total acoustic power, and the acoustic or noise efficiency would compare the different expansion levels. Acoustic efficiency, in a way, will also serve to identify the influence of shock noise on the total intensity.

Acoustic efficiency is defined as:

$$\eta_{acoustic} = \frac{PWL\ overall}{1/2\ \rho_e\ U_e^{\ 3}\ A_e}. \qquad (3\text{-}2)$$

where ρ_e, U_e, A_e are the density, velocity and area in the exit plane of the nozzle. Conventionally, for a circular jet, the easy and widely adopted method for calculating the total power is by integration of SPL on a hemi-

sphere of radius R, which is given by:

$$PWL = \frac{2\pi R^2}{\rho_o c_o} \int_o^{2\pi} \underset{\sim}{p}^2 \sin\theta d\theta \qquad (3\text{-}3)$$

Because of the nonsymmetry of the rectangular nozzle, the above method cannot be used. To facilitate the calculation of the total PWL, integration is performed on a cylindrical surface of radius 30", running co-axial to the jet and extending as far as 52" downstream from the nozzle exit. The same procedure was adopted for the circular nozzle to maintain a consistency in the method of analysis. Ideally, the integration should include some portion of the cylinder upstream of the nozzle, since noise or acoustic waves are bound to propagate in this direction too. However, no measurements were made upstream of the nozzle exit plane.

An assumption made is that the SPL on the cylindrical surface is elliptical[9,17] and the average SPL ($\underset{\sim}{P}_n^2$) is given by:

$$\underset{\sim}{P}_n^2 = \frac{1}{2\pi} \int_o^{2\pi} \frac{P_1^2 P_2^2}{P_2^2 \sin^2\phi + P_1^2 \cos^2\phi} d\phi \qquad (3\text{-}4)$$

P_1^2 and P_2^2 are the SPL along the long and the short axes. This gives the mean SPL as the geometric mean of P_1^2 and P_2^2 and the total acoustic power is:

$$PWL = \frac{1}{\rho_o C_o} \int_o^L \underset{\sim}{P}_n^2 \, 2\pi R \, dx. \qquad (3\text{-}5)$$

The accuracy of this method in calculating the acoustic power is centered around the error associated with the Simpson's rule, the assumption of an elliptical SPL distribution on the cylindrical surface and the interpola-

tion of some intermediate SPL values on this surface. A fixed error with each microphone recording may be due to:

1. Microphone and accessories
2. Digital error - transmission losses and digitization error
3. Signal to noise on the tape recorder.

These errors amount to about $\pm$ 0.4 db. and are known as the fixed errors. These errors are the same for both the circular and rectangular nozzle and hence, as such, only the systemic error is considered. The systemic error due to Simpson's rule and due to interpolation of data points is found to vary between $\pm$ 0.2 and $\pm$ 0.4 db.

Comparison of total power level and the acoustic efficiency for the two nozzles is shown below in Table I.

TABLE I

Pressure Ratio		Underexpanded 29/1	Perfectly Expanded 23/1	Overexpanded 17/1
Sound Power Level PWL db. re 10^{-13} Watts	Circular Nozzle	161.9	161.2	160.6
	Rectangular	161.3	160.2	158.4
Noise η %	Circular	0.27	0.28	0.34
	Rectangular	0.24	0.23	0.21
KE ft lb/sec	Rectangular	$4.26 \cdot 10^5$	$3.4 \cdot 10^5$	$2.44 \cdot 10^5$
Exit Density Ratio $\frac{\rho_j}{\rho_a}$	and Circular	2.2	1.7	1.2

The acoustic efficiencies seem to be quite contradictory for the two jets. Three main observations which can be made are:

1. Noise efficiency decreases with decreasing stagnation pressure for the rectangular jet.
2. Only under the overexpanded case, there seems to be a significant difference in the PWL and hence the acoustic efficiency.
3. The overall efficiencies for the three conditions for the rectangular nozzle seem to be lower than for the circular nozzle.

The error calculations are for individual values, but do not exist when comparing two values for the two nozzles, since the method of data accumulation and analysis is the same.

The rectangular nozzle is designed with the short sides diverging at an angle of 14 1/2° and with this is associated a 3% drop in the theoretical propulsive efficiency. The overall lower efficiency for the overexpanded rectangular jet may be due to the presence of a system of concentrated shocks which rapidly decelerate the jet. Also, since the overexpanded jet minimizes the supersonic core length, the Mach noise is likely to be less. As compared to this, the circular nozzle does exhibit noise due to shock turbulence interaction. This may be attributed to a basic difference in the three and two dimensionality of the shock structure.

3.6 Shadowgraphs

Shadowgraph pictures were obtained to have a clearer understanding of the noise producing mechanisms. Shadowgraphs, as is known, respond to the second derivative of density and as such, the most prominent waves detected are those with the largest derivative and not necessarily with a large sound pressure level. Hence, any finite amplitude waves, which steepen as

they propagate, are detected first. For the rectangular nozzle, shadowgraphs are taken along the two axes. Shadowgraph along the long axis is shown in Fibure 13. The shear layer is thin and grows rapidly as the jet expands. Figure 14 is for the other axis; this shadowgraph is characterized by a thick shear layer at nozzle exit. And although operating under perfect expansion conditions, some internal shocks cannot be avoided. Along the long side of the nozzle is seen a typical Mach wave type radiation, which is not very clear along the short side. Also, in this shadowgraph the near field waves have a larger frequency as compared to Figure 13.

For a better comprehension of the acoustic efficiencies obtained for the rectangular jet, shadowgraphs for the three pressure ratios are compared (Figure 15). This picture basically shows the relative lengths over which the jet decelerates due to turbulent mixing. The rapid deceleration of the overexpanded jet, as stated earlier, is evident from this shadowgraph, and may be related to the low acoustic efficiency. The underexpanded jet passes through a weak system of shocks and takes a longer length to go subsonic.

The overexpanded circular jet (Figure 16) shows a very distinct shock system which extends up to about 10 diameters downstream. Three distinct modes of radiation characterize this picture. The nozzle centered waves emanating from the nozzle lip are spherical in shape and seem to be dipole type of radiation. The second type is either due to shear layer instability or due to supersonically convecting eddies. This type of waves were first studied by Phillips, Ffowcs Williams and Ribner and all viewed the noise generating mechanisms as supersonic eddies. However, recently Tam

and Liu have shown these to be due to shear layer instability.

In an attempt to associate these waves with the eddy Mach waves, the eddy convective velocities are computed. The mean eddy convective velocity was found to vary from 65 to 80% of the nozzle exit velocity, for the three expansion conditions. The corresponding values for the rectangular nozzle vary between 70 and 80%. This is in general agreement with other experimental observations[13,14] which indicate similar values. Eddy Mach angles for waves along the long side seem to correlate quite well with the far field directivity angle. However, along the short side, no distinct Mach waves are seen, and still the far field directivity angle is of the same order. Directivity, besides being a function of Mach angles, is affected by refraction, which is quite prominent along the long axis.

The third type of radiation are the spherical acoustic waves which originate where the shock cells interact with the shear layer. These waves propagate normal to the jet axis, and do not interfere with waves originating from other sources. These waves are distinctly observed for the circular jet, whereas for the overexpanded rectangular jet, even with the presence of a concentrated shock system, practically no spherical waves are seen to emanate.

CHAPTER IV

HIGH TEMPERATURE ANALYSIS (4900°R)

Hubbard and Lassiter[20] first investigated the effect of density on jet noise by conducting a series of experiments with gases of different molecular weights (air, helium, freon). It is, however, still not very clear whether a cold jet using various gases does simulate a hot jet, whether heat transfer influences noise generation or radiation.

The main purposes of operating the high temperature jet were:

1. A temperature around 4900°R (T_{o5}) more or less simulates rocket exhaust temperatures. Also, with such high exit temperatures, a large density ratio between the ambient and the jet is obtained, and its effect on jet PWL, directivity and shock noise could be studied.
2. Density and temperature variations are some of the parameters to be used for formulation of scaling laws.

For the rectangular nozzle, the low temperature analysis did not show significant contribution by shock shear layer interaction. The effect of temperature on shock noise could be estimated from such high temperature analysis.

Such a high temperature of 4900°R was achieved by "tailoring" and without mixing gases in the driver section. Also, a highly overexpanded case was worked out, which, besides giving a system of strong shocks, gave an exit density variation of 0.325 $(\frac{\rho_j}{\rho_a})$ as compared to 1.2 for the low temperature jet. The underexpanded case was operated at a moderately high stagnation pressure of 26 atmospheres.

4.1 Directivity Patterns

The directivity patterns are once again calculated for the three

expansion conditions. Figure 17 compares three testing conditions for the circular jet of stagnation temperature 4900°R. The overexpanded jet seems to have a maximum far field directivity of about 70°, which decreases to about 60° for the underexpanded jet. For all the expansion levels, the far field directivity seems to be focused in a region 14 to 17 nozzle diameters downstream. As compared to this, the low temperature directivity angles were between 44° and 53°.

For the rectangular jet, the directivity patterns were again plotted along the two major axes of the nozzle. The basic trend regards the difference in directivity along the two axes as follows: more directional along the long axis than the short; however, there is seen to be an overall increase in directivity. Along the long axis, the directivity angle varies between 66° and 70°, whereas along the short axis, the angle varies between 61° and 64°. Here also is observed an increase in directivity from the low temperature analysis. Also, the maximum directivity seems to be focused in a region 10" to 14" from the nozzle exit, along both the axes. The low temperature directivity, on the other hand, is seen to focus at a lesser distance, indicating either a shift in the region of transition to subsonic flow at high temperature, or this shift may be due to an apparent increase in the eddy convective velocity.

The increase in directivity angle is to be expected at higher temperatures because of the increase in convective velocity and also a greater refraction of the sound sources generated within the jet, due to a larger density gradient between the jet and the ambient. Even though the exit jet to ambient density ratio for the overexpanded jet is 0.325 as compared to 0.5 for the perfectly expanded jet, the difference in directivity angles is quite small. This goes to say that for a given jet exit temperature, a

variation in jet exit density by a variation in jet stagnation pressure does not greatly affect the directivity, i.e., presence of shock structure does not significantly change the directivity.

All the directivity curves plotted so far are for the overall frequency; directivity in different frequency bands have not been considered here, but could be computed by introducing digital band pass filters in the main program which calculates the SPL.

4.2 Ellipticity

Again the ellipticity function is plotted for the rectangular jet as function of axial distance. Figure 18 shows such ellipticity on a cylindrical surface of radius 30". Maximum ellipticity is found to vary with distance from nozzle exit for each of the three cases. It is observed that these curves are somewhat different than from the low temperature analysis, where a minimum of 3 db ellipticity was maintained along the axial length of the jet. Ellipticity, which is a function of nozzle aspect ratio, is affected by the jet aspect ratio some distance downstream, since increasing jet aspect ratio would scatter and refract sound sources more along the long axis than the short axis. The maximum ellipticity is found for the under and overexpanded jets, which basically shows the influence of shocks on directivity.

The jet, at various sections of its length, is characterized by different frequency emission, and to see this effect Figure 19 is plotted, which gives the intensity at different frequencies along the long axis of an underexpanded jet as a function of axial distance. It is observed that the noise intensity distribution shifts towards lower frequency with distance downstream. Low frequencies in the range 2-8 kc dominates in the

region of maximum intensity. The turbulence scale which increases with distance is mainly responsible for this observed frequency shift.

4.3 Shadowgraphs

At this temperature (4900°R), a high level of density variation does not produce shadowgraphs to be very informative, for

1. The jet internal structures are not very well defined.
2. High level of turbulence in the mixing layers obscure the origin of the near field wave forms.

From Figure 20, which is for a perfectly expanded rectangular jet, is observed a strong eddy Mach wave type radiation which gives an eddy convective velocity of about 49% of the jet exit velocity. A similar convective velocity was observed for the overexpanded case. For the circular nozzle too, the eddy convective velocity is lowered to about 55%. Thus, the high temperature jet exhibits a lower percentage of exit velocity, as compared to the low temperature jet where the mean velocity was around 70 to 80%.

Figure 20 shows an increase in Mach angle with distance, and also these waves tend to become spherical as they mix.

Figure 21 shows an overexpanded circular jet with stagnation pressure of about 15 atmospheres; here no strong shock structures are visible nor are any spherical waves. The turbulent mixing observed is more intense than for low temperatures, which suggests temperature and density do have some effect on the mixing process. There are also observed some instabilities (Taylor instabilities) due to a lighter gas driving a heavier gas.

Table II is for the far field directivity angles correlated with the eddy Mach angles measured from the shadowgraphs. This is for the rectangular jet where the Mach angles were defined quite well along the long side

of the nozzle.

TABLE II

Pr. Ratio	Low Temperature (1350°R)			High Temperature (4900°R)		
	17/1	23/1	29/1	15/1	23/1	26/1
Mach Angle θ_M	40±3	37	35	30	28	--
Directivity Angles θ_s	52±2	53	56	61	64	65
$\theta_M + \theta_s$	--	90	91	91	92	--

4.4 Acoustic Effieiency and Total Power Level

The method so far used for calculation of acoustic power and efficiencies may not be an ideal or an exact one, but could be used to compare the two nozzles, since all the errors associated in calculation and measurements are almost the same for both the nozzles.

The same procedure is applied for calculation of total power as was used for the low temperature analysis. Table III gives the overall power level and the acoustic efficiency for both the circular and the rectangular jets operating at a stagnation temperature of 4900°R.

The overall performance of the high temperature circular jet shows a considerable increase in the acoustic efficiency with respect to the low temperature. The overexpanded jet exhibits the maximum acoustic efficiency, even when it has the lowest KE, showing the dominance of shock-shear layer interaction.

The rectangular nozzle, on the other hand, has a lower PWL and hence a lower acoustic efficiency compared to circular nozzle. Here, the underexpanded and the overexpanded jets show an increase in shock noise or an

TABLE III

Level of Expansion		Underexpanded	Perfectly Expanded	Overexpanded
Pr. Ratio		26/1 Deviation	23/1	15/1
PWL in db. re 10^{-13} Watts	Rectangular	166.1	165.2	163.4
	Circular	168.2	168.0	166.5
$\eta_{acoustic}$ in percent	Rectangular	0.43	0.36	0.38
	Circular	0.67	0.73	0.77
KE of Jet at Exit ft lb/sec		7.23×10^5	6.4×10^5	4.27×10^5
Density Ratio $(\frac{\rho_j}{\rho_a})$		0.59	0.52	0.325

increase in eddy Mach wave noise for an increase in the length of supersonic core. For the overexpanded case, even though the KE is 2/3 of perfect expansion, the noise efficiency is about 9% higher.

The increase in acoustic efficiency for the low temperature for both the nozzles is mainly due to an increase in exit velocity, which has nearly doubled. The KE, on the other hand, has increased by a factor of 1.8 on an average.

CHAPTER V

INTERMEDIATE TEMPERATURE ANALYSIS (2900°R)

The main purpose of the intermediate temperature analysis is to verify the independence of the OPWL equation for temperature. Analysis at this temperature was only carried out for the circular nozzle.

Here again, three levels of expansions with stagnation pressures of 14, 23, and 27 atmospheres were examined. Using air and argon, a shock Mach number of 2.6 (with stagnation temperature 2900°R) gave test time of about 25 msec.

To verify the directivity angles obtained for the two extreme temperatures, the directivity patterns were plotted at this temperature, and the directivity angles found.

Figure 22 compares the directivity pattern for the over, under and perfectly expanded conditions; the directivity angles are found to vary between 52° to 58°. Similar angles for the low temperatures varied from 44° to 51° and for high temperature from 60° to 70°. This again shows the influence of temperature and hence density on directivity. The directivity angle increases with increasing temperature.

5.1 Acoustic Efficiency and OPWL

The same procedure was followed as outlined for the low temperature for the calculation of acoustic power and efficiency. Table IV contains the values obtained for the three expansion levels.

TABLE IV For Circular Nozzle

Level of Expansion	Underexpanded	Perfectly Expanded	Overexpanded
Pr. Ratio	27/1	23/1	14/1
OPWL in db. re. 10^{-13} Watts	164.8	164.4	162.8
% Efficiency	0.389	0.416	0.472
Jet KE ft lb/sec x 10^5	5.7	4.86	2.96
Exit Density Ratio $(\frac{\rho_j}{\rho_a})$	1.42	1.15	0.8

Here again, it is found that the overexpanded jet has the highest acoustic efficiency, and contribution due to shock shear layer interaction could be significant.

5.2 Scaling Laws

The basic parameters governing the noise production in a supersonic jet are the Mach number, the pressure, temperature (stagnation) and the molecular weight. With these parameters one should be able to predict the overall sound power level, and to do this, some preliminary scaling laws based on experimental results are to be developed. For an exit Mach number of 2.74, at a particular stagnation temperature (1350°R or 4900°R), the only variation in jet operating condition is the stagnation pressure.

Since for both the circular and rectangular nozzle the PWL increases with stagnation pressure, a relation involving stagnation pressure is

worked out. The overall power level is plotted as a function of $(\frac{p_o}{p_{o\ ref}})^n$. At one stagnation temperature, the OPWL is expected to vary according to:

$$OPWL = OPWL_{ref} + 10 \log (\frac{p_o}{p_{o\ ref}})^n \qquad (5\text{-}1)$$

where $p_{o\ ref}$ is taken here as for the perfectly expanded case, since it is constant for a given exit Mach number. By determining the slopes of these curves, the value of the exponent n is determined. This value for low temperature was found to be 1.33 for rectangular jet and 0.58 for circular jet. At the higher temperature this value for the rectangular jet decreases slightly to 1.1, but for the circular it remains more or less constant at 0.6 (See Figure 23).

The slopes of these curves to some extent indicate the influence of shock shear layer interaction, since the only variable parameter is the stagnation pressure, which affects the level of expansion. The maximum difference in the OPWL for the two nozzles at the two temperatures is observed for the overexpanded jet.

For the circular nozzle, the independence of the value of n for low and high temperature may suggest the independence of OPWL equation with temperature. To verify this, another intermediate temperature (2900°R) is experimented.

Once again a value of n approximately equal to 0.6 was obtained. Therefore, for the circular nozzle, a scaling law was formulated which gives the sound power level as a function of stagnation pressure:

$$OPWL = OPWL_{ref} + 10 \log (\frac{p_o}{p_{o\ ref}})^{0.6}. \qquad (5\text{-}2)$$

The next step was to determine the sound power level of the perfectly expanded jet as a function of the stagnation temperature. Figure 24 shows

that such a relation is linear, and an equation is determined for calculating the sound power level at any stagnation temperature for an exit Mach number 2.7.

$$OPWL_{perf} = (1.92 \times 10^{-3})\ T_{stag.} + 158.8 \text{ db.} \qquad (5\text{-}3)$$

This equation in more general terms can be written as

$$OPWL = [(1.92 \times 10^{-3})\ T_{stag.} + 158.8] + 10 \log_{10} \left(\frac{P_{stag.}}{23}\right)^{0.6} \qquad (5\text{-}4)$$

for an exit Mach number of 2.74, which gives a stagnation pressure for perfect expansion as 23 atmospheres. $P_{stag.}$ is in atmosphere. This equation, however, predicts the sound power level on a cylindrical surface of radius 21 diameters and extending about 39 diameters from nozzle exit. Also the above equation was developed from only three distinct stagnation temperatures and needs to be verified at some other values. This equation holds true for an exit Mach number of 2.74, and for different Mach numbers the exit area is to be changed.

Scaling for acoustic efficiency is another criterion which may be considered here. This is considered only for the circular jet.

The Table below gives the acoustic efficiencies* for the three expansion levels at the three stagnation temperatures.

TABLE V

	1350°R	2900°R	4900°R
Over Expanded	0.344	0.47	0.77
Perfectly Expanded	0.28	0.42	0.726
Under Expanded	0.27	0.39	0.67

* percentage

From this table, it is observed that the acoustic efficiency increases as the stagnation pressure decreases. At each temperature the overexpanded jet is the most noisy. It may be surprising to note that the perfectly expanded jet is noisier than the underexpanded jet, which is not the case with the rectangular nozzle.

For the three stagnation temperatures worked, the only expansion condition at which the stagnation pressure was held constant is the perfect expansion condition. Figure 25 is a graph for the acoustic efficiency versus stagnation temperature (for perfectly expanded conditions). With three points, however, it is difficult to ascertain whether the graph represents a linear relationship or not.

However, the acoustic efficiency is given by $\eta_{acoust} = \frac{OPWL}{KE}$.

Now $PWL_{perf} = 10 \log (PW) + 130$ db. (5-5)

PW = integrated acoustic power level on cylindrical surface.

Also $PWL_{perf} = (1.92 \times 10^{-3})\ T_{stag.} + 158$ db. (5-3)

From (5-3) and (5-5) we obtain:

$$10 \log PW = (1.92 \times 10^{-3})\ T_{stag.} + 28.8 \text{ db.} \quad (5\text{-}6)$$

$$PW = 10^{\frac{[1.92 \times 10^{-3}\ T_{stag.} + 28.8]}{10}}.$$

KE is given by $KE = 1/2\ (\rho\ A\ U^3)_e$.

$\rho_e = \frac{P_e}{R\ T_e}$. ρ_e for the perfectly expanded case is assumed to be one atmosphere, and $T_e \propto T_o$ for a given Mach number.

$$\eta_{acoustic} = \frac{C}{\sqrt{T_{stag.}}}\ 10^{[(1.92 \times 10^{-4})\ T_{stag.} + 2.88]} \quad (5\text{-}7)$$

The value of C can be calculated knowing the acoustic efficiencies and the stagnation temperatures. An average value comes out to be (7.8×10^{-3}).

$$\eta_{acoustic} = \frac{8 \times 10^{-3}}{\sqrt{T_{stag.}}} 10^{[(1.92 \times 10^{-4}) T_{stag.} + 2.88]} \qquad (5\text{-}8)$$

Thus for an exit Mach number of 2.74, acoustic efficiency can be calculated for any stagnation temperature.

5.3 Auto and Cross-correlation

The near field is characterized by supersonically travelling eddies which, as is found, influence the directivity to some extent and also the near field intensity spectra. Shadowgraphic observations show these near field waves to be of high intensity which, however, are not very well correlated in the frequency spectra.

In order to understand these sources, their velocity, size and frequency should first be estimated. This could be achieved by correlating the near field pressure fluctuations. For the present report, this technique was just developed and not explored fully, but is to be used on later work.

In dealing with near field pressure correlation, it is necessary that the microphones be located as close to the jet as possible so as not to pick up radiation from any other sources downstream or upstream. For the two microphones located about 12" offstream and 6" apart, the auto and cross-correlation curves are shown in Figure 5. The cross correlation curve is rather meaningless since the distance between the microphones is too large. The maximum cross-correlation is seen to be about 0.22, which should, however, increase as the distance between microphones is reduced. Knowing the distance between the microphones and the time after which the maximum cross-

correlation occurs, one is able to estimate the average eddy convective velocity. The eddy size could be estimated from the auto-correlation.

Recalling the shift in frequency as a function of axial distance, it is observed that higher frequencies are radiated at a sharper angle to the jet axis, which could be due to:

1. High frequency wave form is scattered more by density gradients than low frequency.
2. The convective velocity of the eddies responsible for high frequency radiation may be larger than the mean eddy velocity. This is because of the velocity gradient in the mixing layer, and also the eddy sizes vary from the jet boundary to the potential core.

To determine the variation of eddy sizes in the mixing layer and their frequencies, it is necessary to correlate the pressure fluctuations within the jet at different centre frequencies.

Still another method by which the source origin and radiation could be visualized is by cross-correlating the pressure fluctuation within the jet to the acoustic pressure fluctuation outside.

Mollo-Christensen[22] showed some space-time correlation of acoustic pressure fluctuation at different frequency band widths for some near field measurements. This was to show that turbulence is composed of different frequencies which retain their phase over a few jet diameters.

CHAPTER VI

CONCLUSIONS

The conclusions which can be inferred from the data analysed for the circular and the rectangular jets are:

For the low and high temperature analysis, it is found that the OPWL for the three expansion conditions for the rectangular jet is lower than that for the circular jet. The difference is significant for the high temperature case and is maximum for the overexpanded jet.

The variation in the local sound pressure level for the two jets is associated to a basic change in the geometry of the nozzles. The design for the same exit Mach number leads the rectangular nozzle to have a higher surface to volume ratio as compared to a circular nozzle, and hence more entrainment flow.

As observed from Tables I and III, the overall power level for the rectangular jet increases with increase in stagnation pressure, which is mainly due to an increase in KE. The contribution due to shock shear layer interaction can be only seen from the acoustic or noise efficiency. For the rectangular jet at low temperature, the increase in acoustic efficiency with stagnation pressure shows no contribution by shock noise. On the other hand, the circular nozzle shows an increase in acoustic efficiency, which is mainly due to presence of shocks.

At the high temperature, both circular and rectangular nozzles show increased acoustic efficiencies at off design conditions; however, the increase is greater for the circular nozzle than for the rectangular nozzle. One conclusion which can be made from this analysis is that the acoustic efficiency increases with increase in stagnation temperature.

In comparing the two nozzles, it is evident that the rectangular noz-

zle is indeed quieter than the circular nozzle. The rectangular nozzle is more effective under overexpanded conditions, and a factor of 1.6 in acoustic efficiency at low temperature and about 3 at high temperature is observed. The low acoustic efficiency for the overexpanded rectangular jet is related to a rapid deceleration of the jet through a system of strong shocks. This is not observed at high temperature, where the level of expansion was more or less the same; however, at this high temperature, density seems to have some influence. A light gas driving a heavier gas may result in a very unstable shear layer due to Taylor instabilities.

For both the circular and rectangular nozzles, the effect of temperature showed an increase in the directivity angle at high temperature, which is correlated to an increase in eddy convective velocity, rather than refraction due to density gradients, which seems to play a secondary role.

With the rectangular nozzle is associated an ellipticity function, which for the low temperature was maintained at a minimum of 3 db. along the axial length of the jet. However, at the high temperature the off design conditions seem to affect the directivity and hence the ellipticity. A maximum ellipticity of about 7 db. at low temperature is reduced to 5.5 db. at the high temperature. This shows the influence of temperature on the jet aspect ratio, which influences ellipticity.

The low temperature overexpanded jet showed a difference of about 2.6 db. in the OPWL between the two nozzles. However, at this condition, for the rectangular nozzle, a difference of about 8 db. between the maximum and minimum noise direction is observed. Hence, a suitable orientation of the nozzle could cause a considerable reduction in the noise level. The rectangular nozzle seems to be very effective under overexpanded conditions.

However, with this nozzle is associated a reduction of 3% in the theoretical propulsive efficiency.

The scaling laws, which are in the preliminary stages, were developed for the change in the OPWL as a function of stagnation pressure. For the circular nozzle, additional scaling was done for temperature and acoustic efficiency. These scaling laws now need to be verified for additional temperatures. Also, these laws are for an exit Mach number of 2.74 and an additional dependence will be developed as a function of Mach numbers. For the variation of OPWL with stagnation pressure, the scaling factor (n) shows the influence of shock-shear layer interaction on the total noise level. This value of n is 0.6 on an average for the circular nozzle and varies from 1.1 to 1.3 for the two temperatures for the rectangular nozzle.

The scaling laws predicted here are preliminary and are to be verified with additional data. Also, this work should initiate further work on the potential use of the rectangular nozzle as a noise suppressor and as a model for better comprehension of noise generating mechanisms.

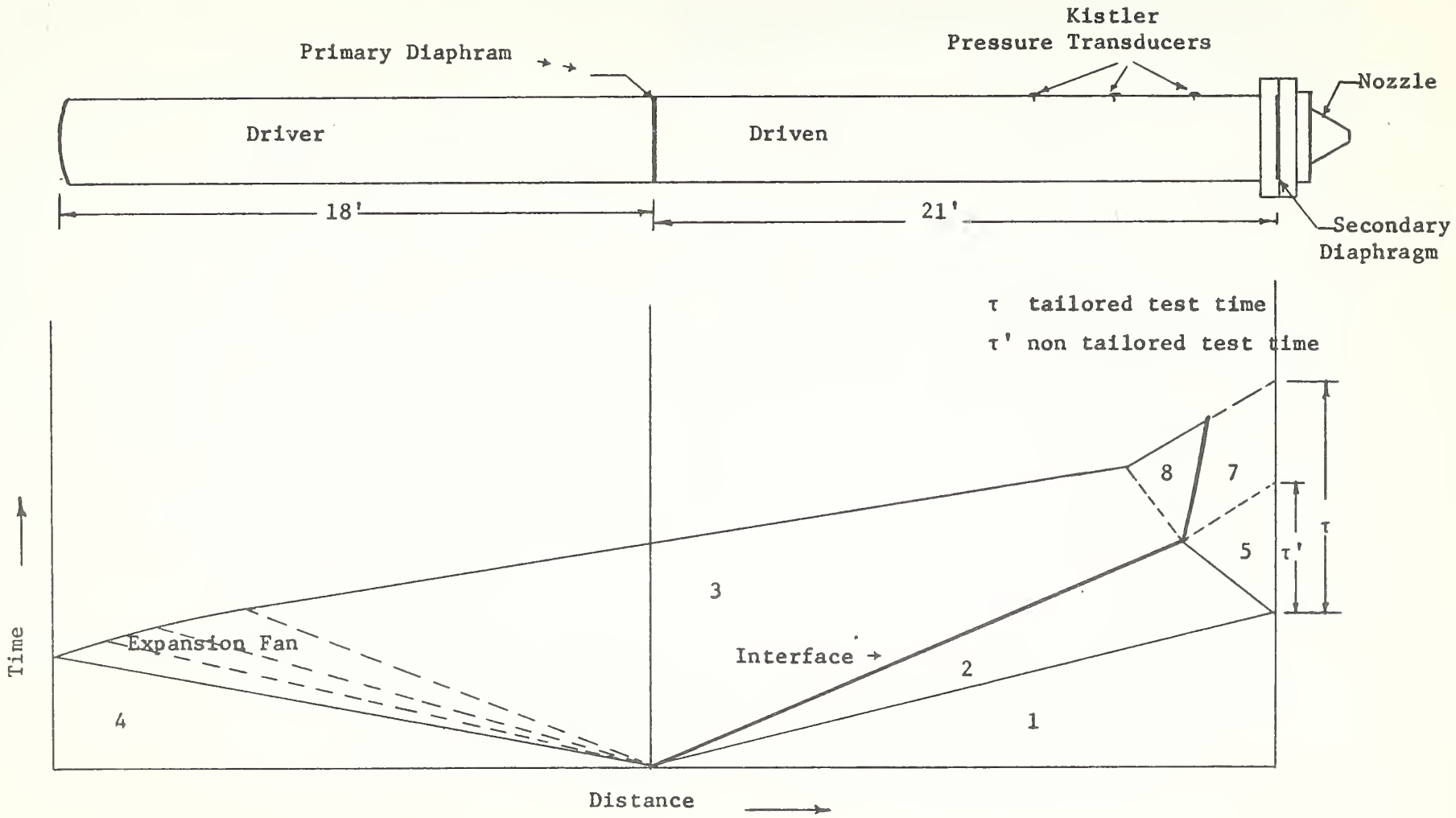

Figure 1: Time distance history in shock tunnel

OSCILLOSCOPE TRACES SHOWING SHOCK SPEED AND TEST TIME

Low Temperature

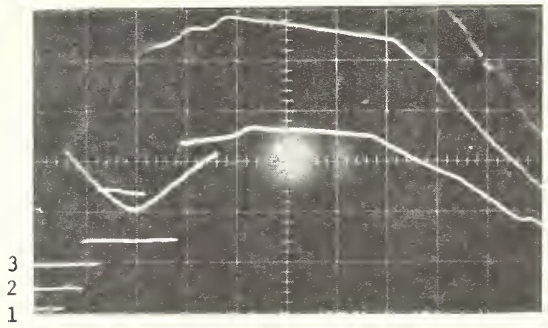

1,2,3 Sweep Speed 5 millisec/cm

High Temperature

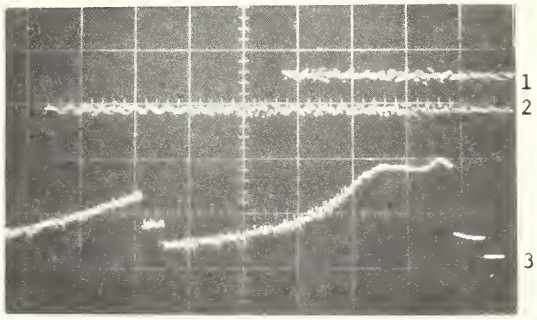

1,2 Sweep Speed 0.2 millisec/cm

3 Sweep Speed 5.0 millisec/cm

OSCILLOSCOPE TRACES SHOWING RESPONSE OF THE B&K MICROPHONES

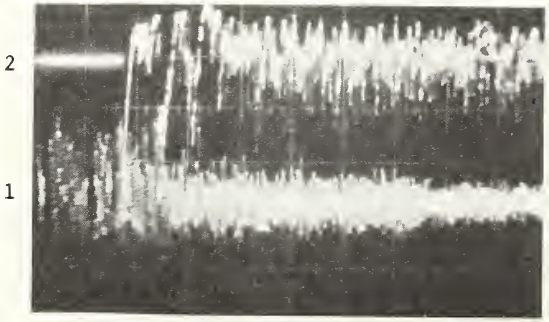

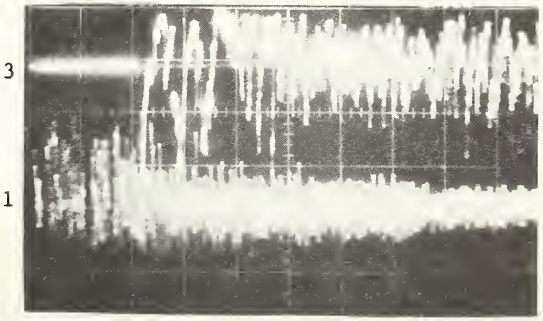

1 - Trigger transducer located at nozzle exit 2 volt/cm

2 - B&K microphone 1 volt/cm
18 inches from centerline
27 inches downstream

3 - B&K microphone 1 volt/cm
18 inches from centerline
36 inches downstream

Figure 2

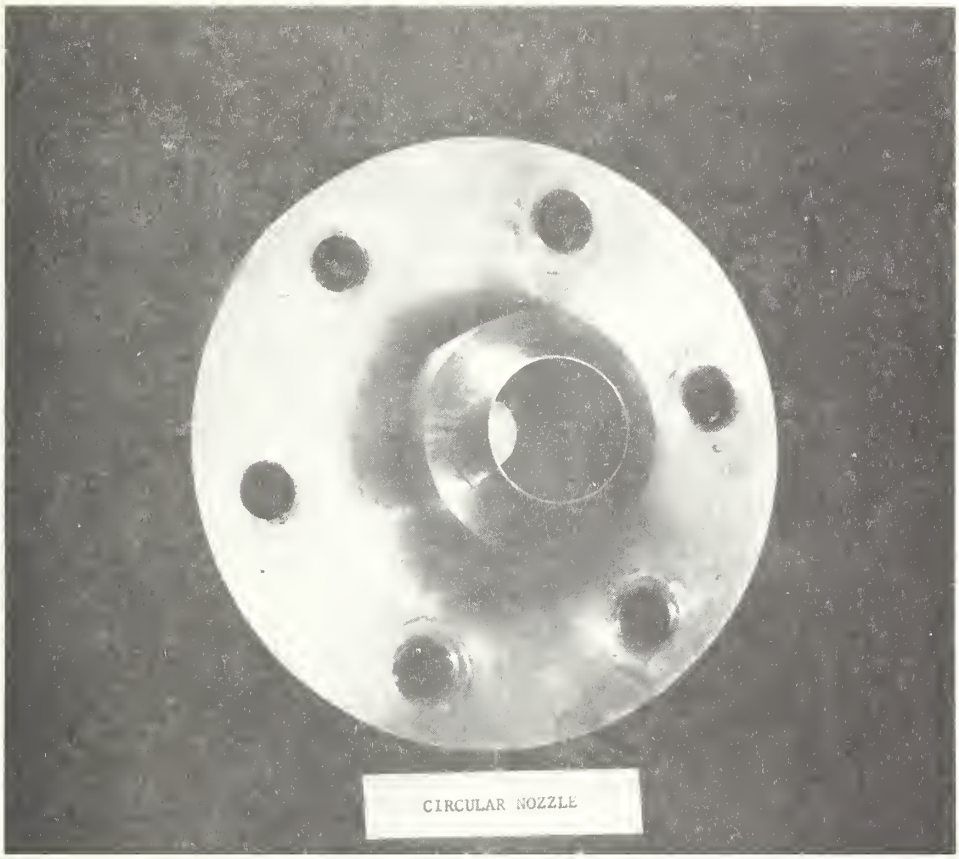

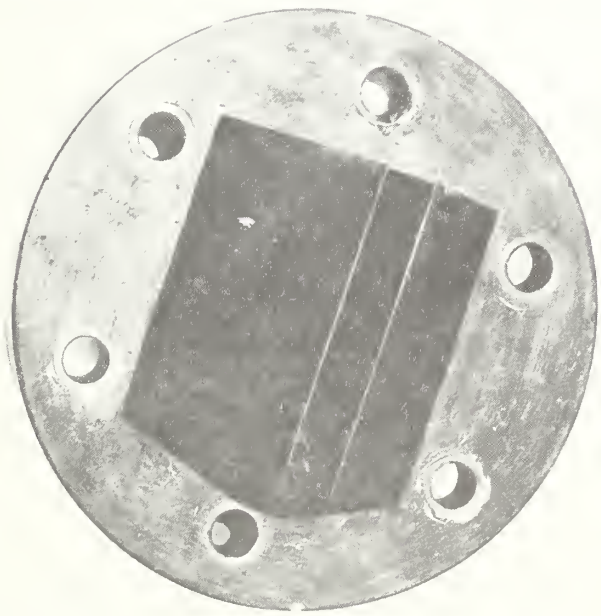

SLOTTED NOZZLE

Figure 3

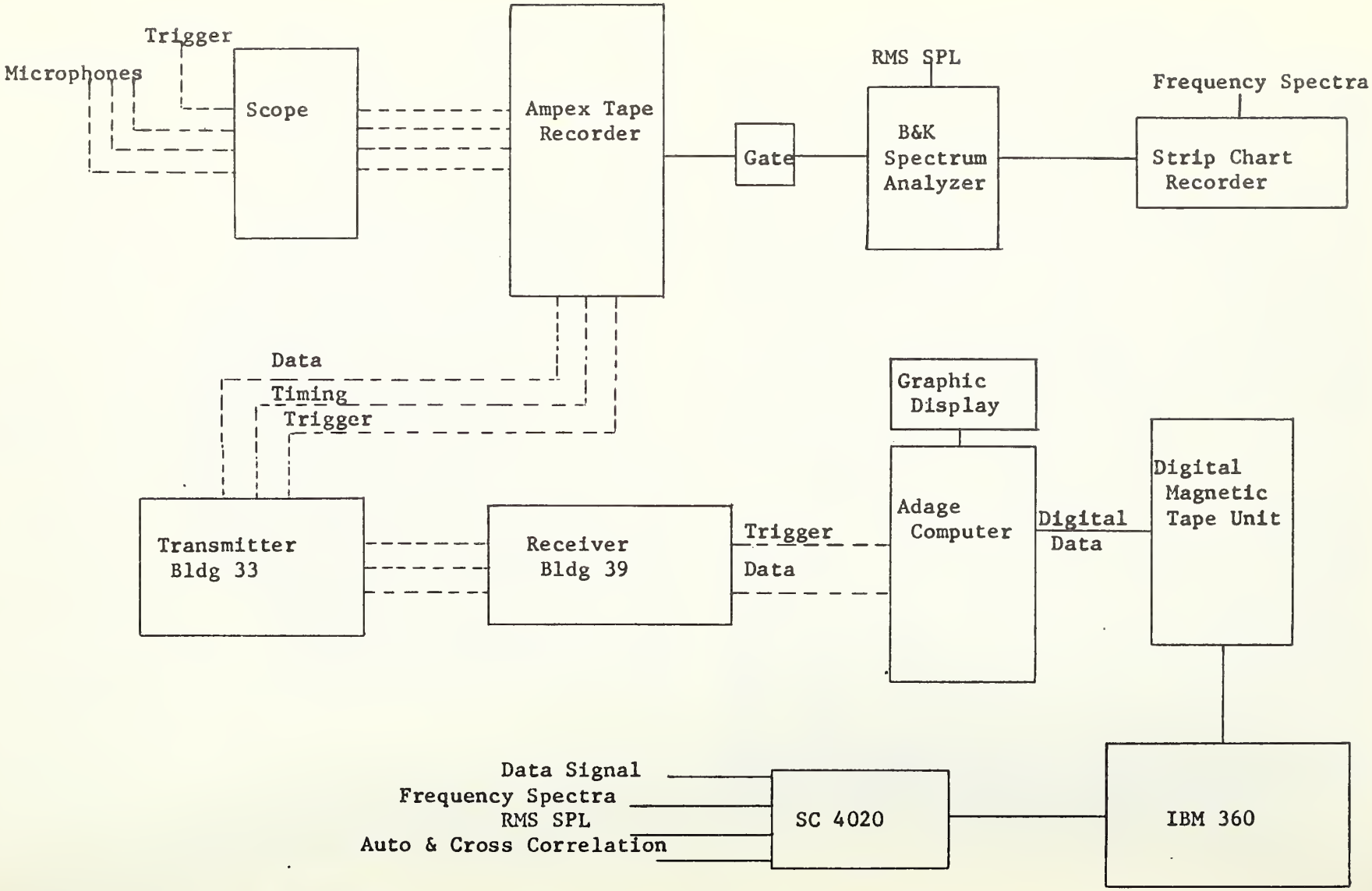

Figure 4
SCHEMATIC OF DATA ACQUISITION AND REDUCTION SYSTEM

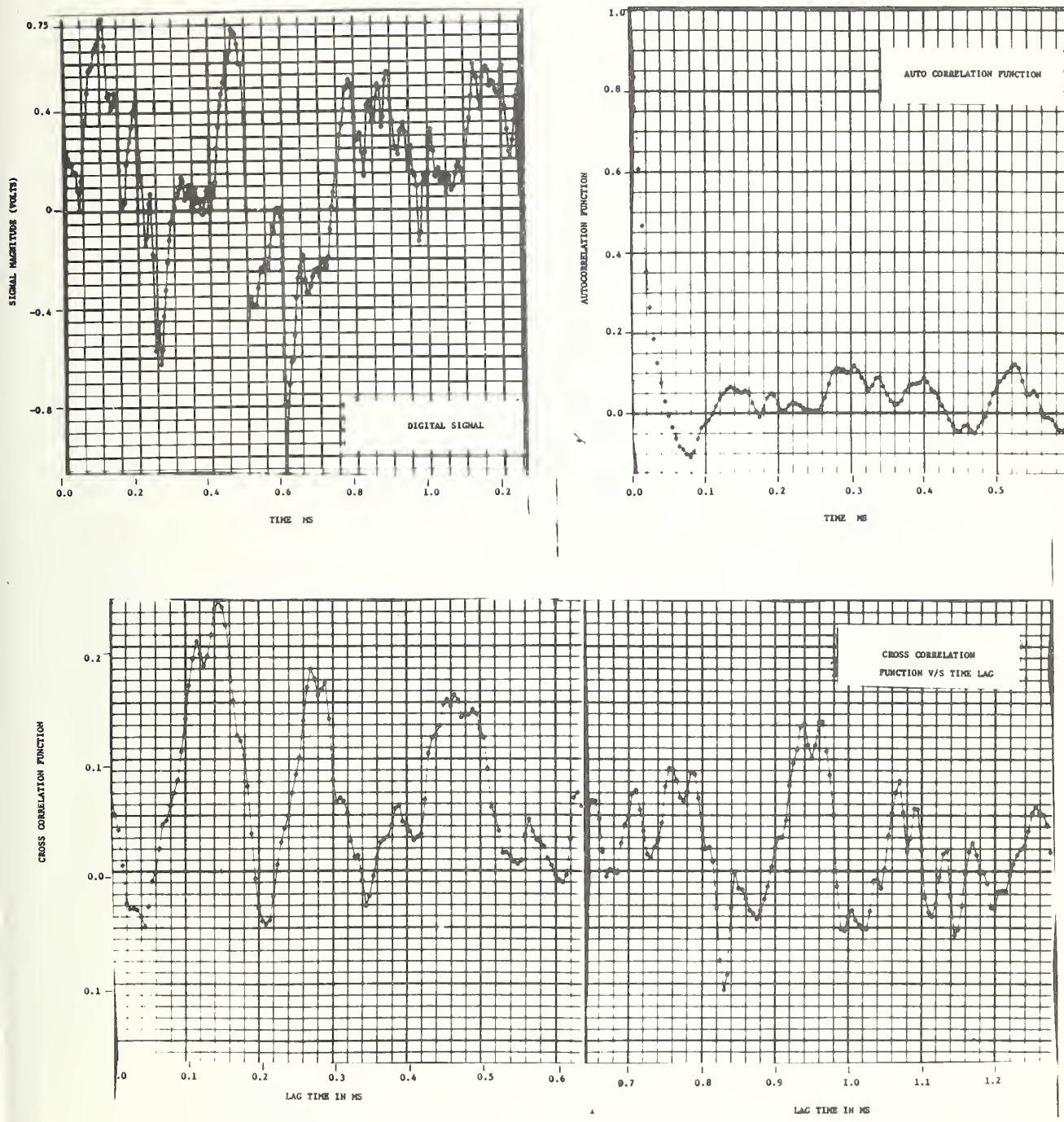

Figure 5: Digital signal; auto and cross correlation functions.

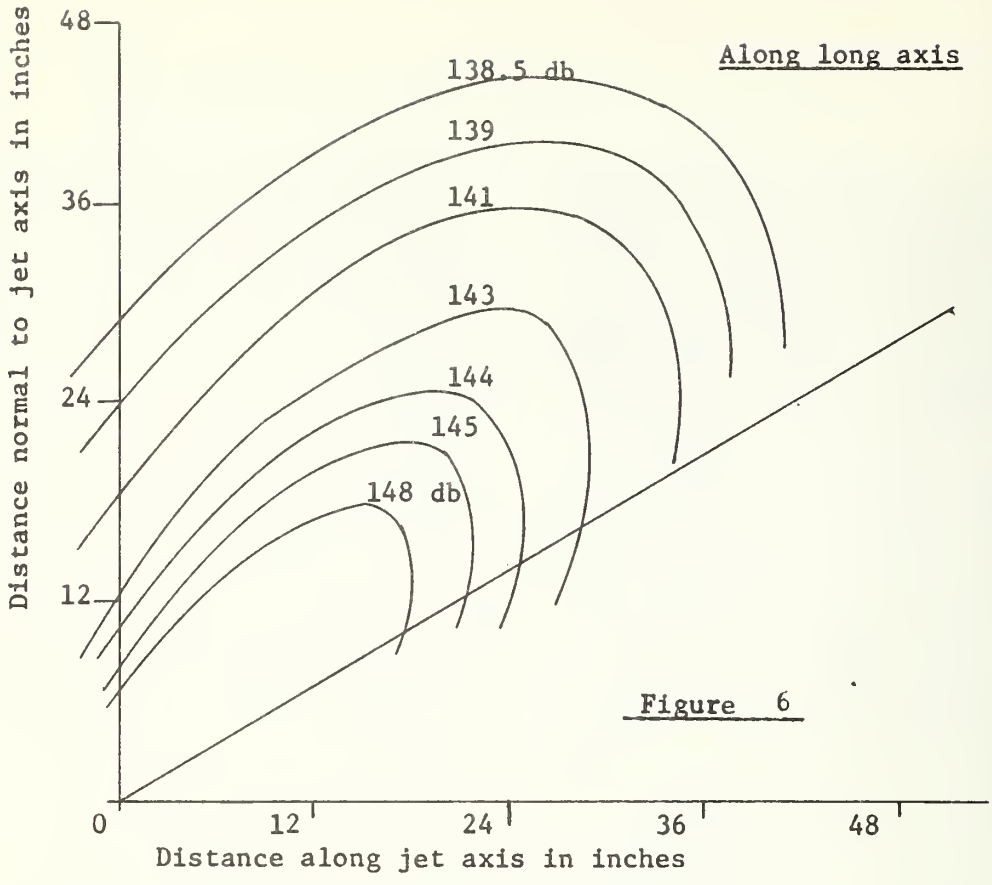

Figure 6

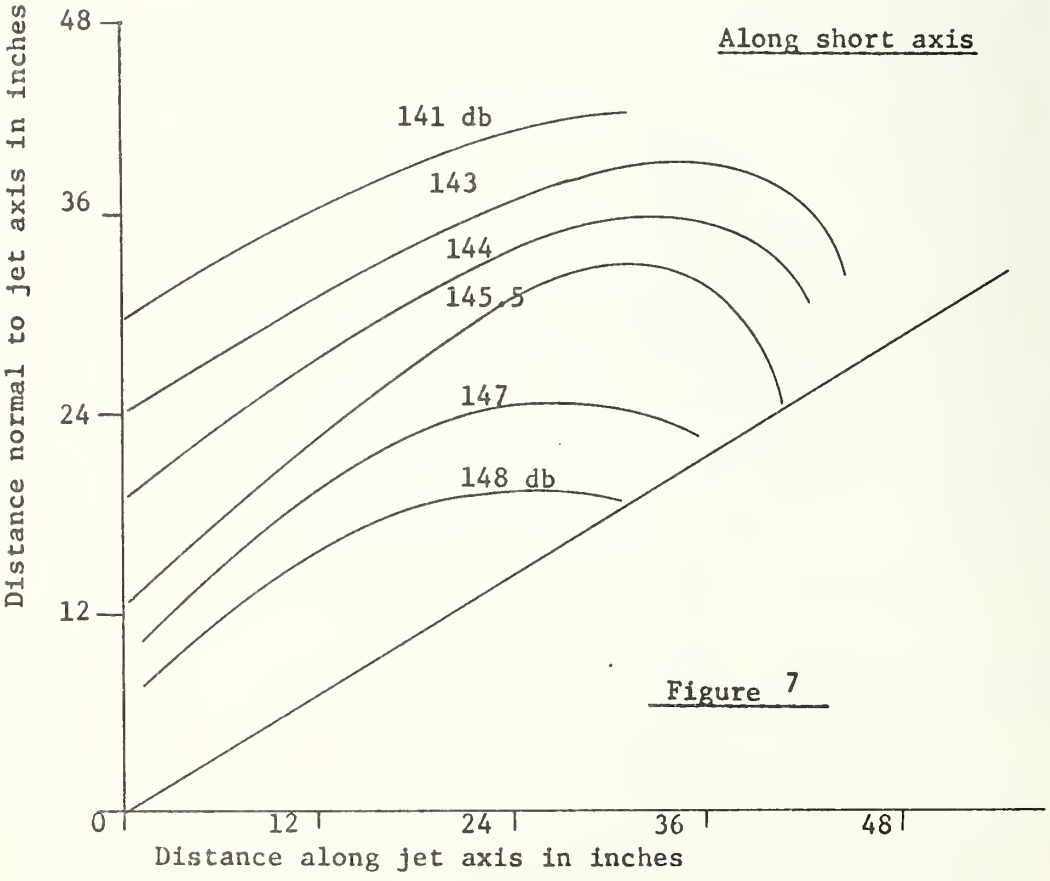

Figure 7

DIRECTIVITY PATTERN FOR PERFECTLY EXPANDED JET (LOW TEMP.)
IN THE TWO NOZZLE AXIS

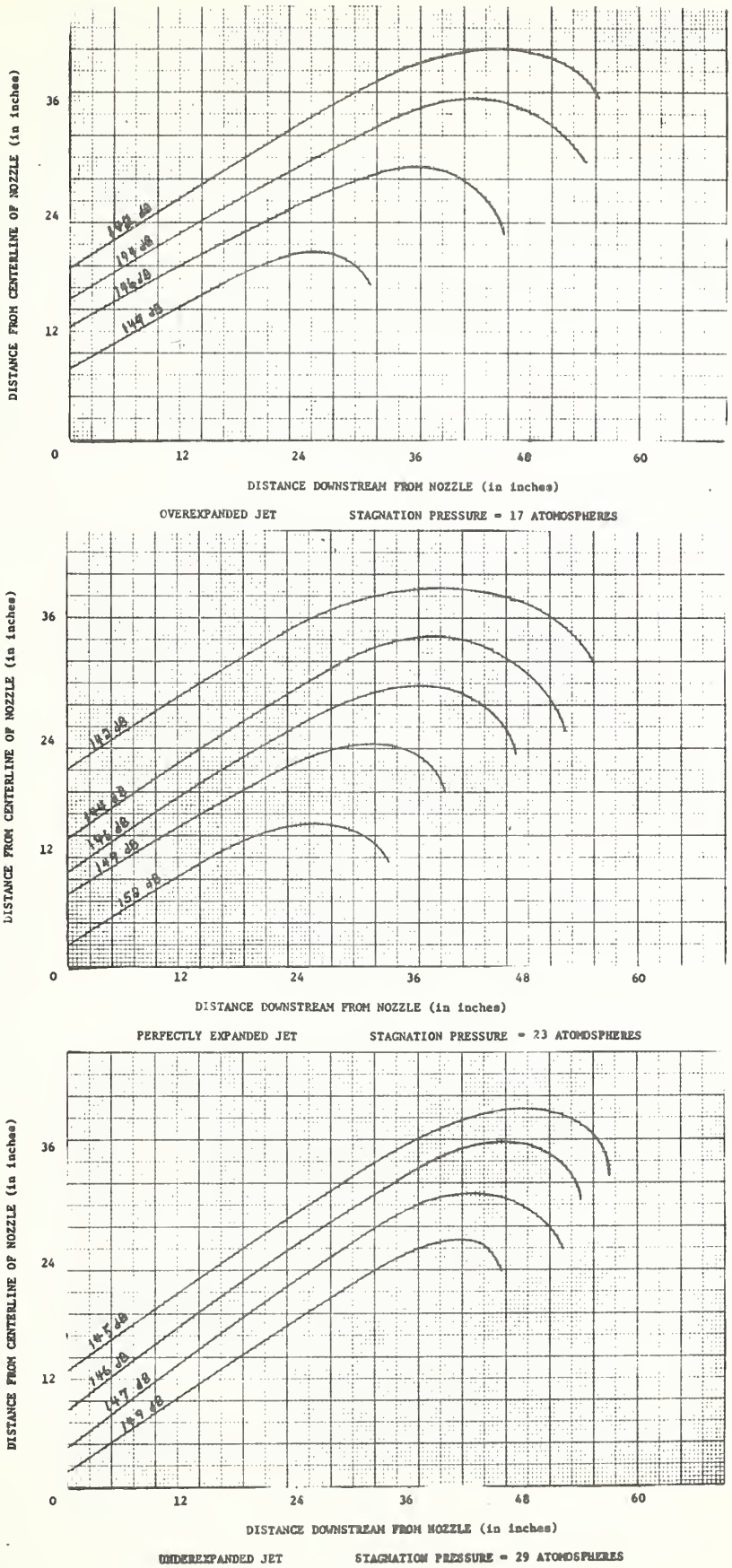

Figure 8

DIRECTIVITY PATTERNS OF THE CONTOURS OF CONSTANT dB LEVELS FOR A STAGNATION TEMPERATURE OF 1350 °R

Figure 9: ELLIPTICITY AS A FUNCTION OF AXIAL DISTANCE ON A CYLINDRICAL SURFACE OF RADIUS 36" COAXIAL TO JET

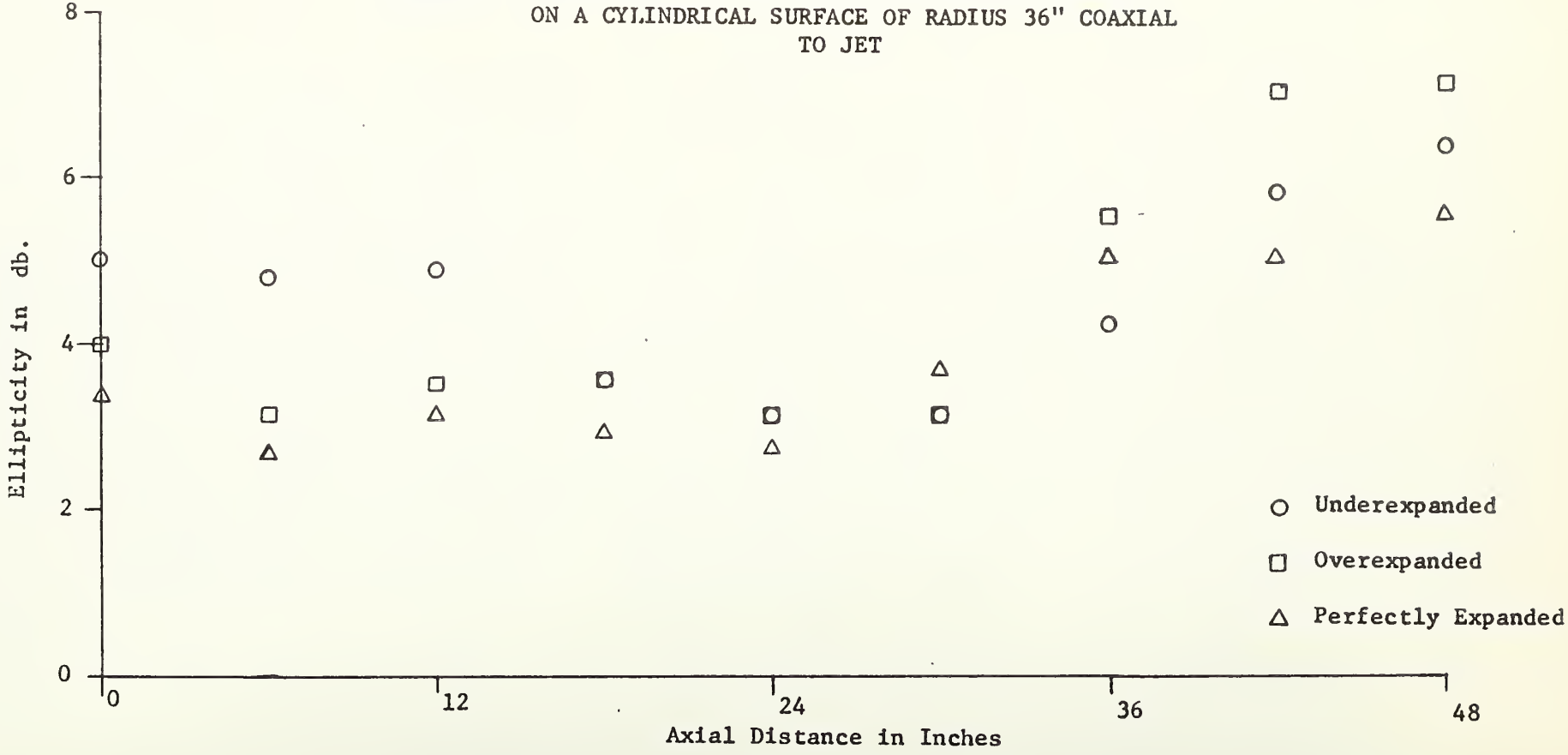

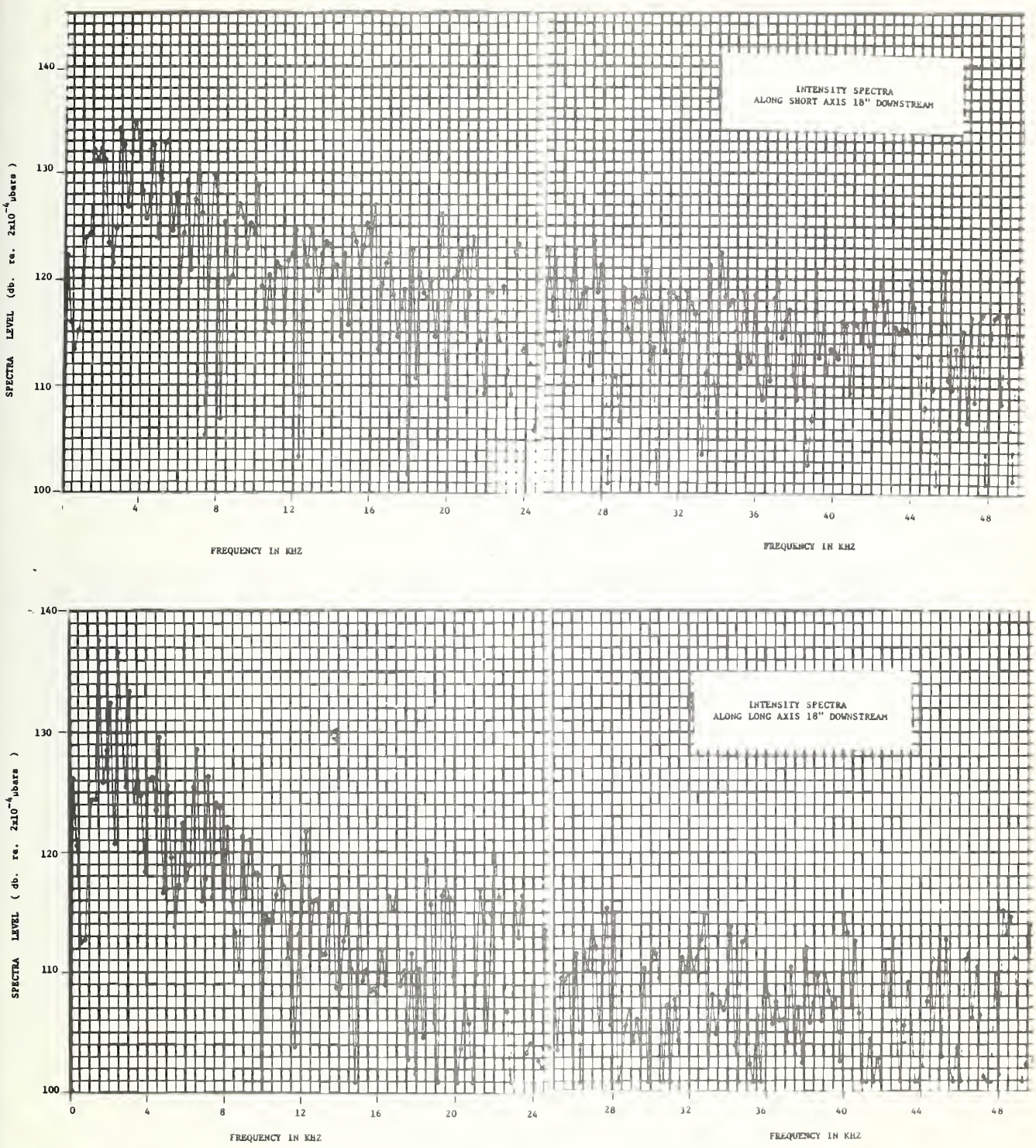

Figure 10: Characteristic frequency spectra along the long and the short axes.

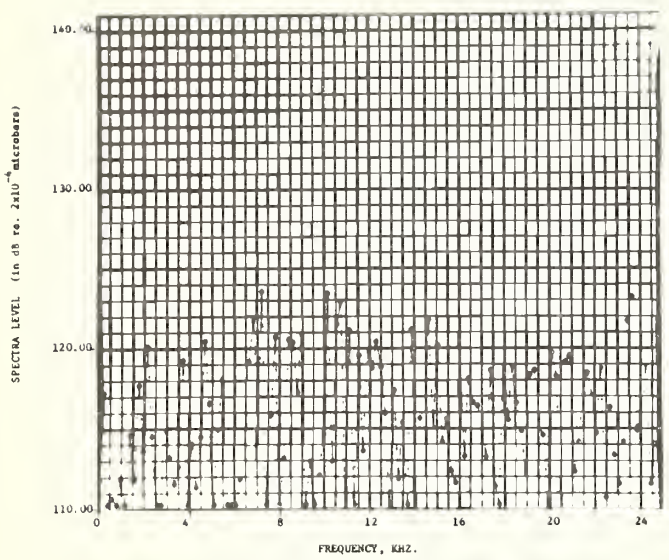

24 inches from centerline, 18 inches downstream

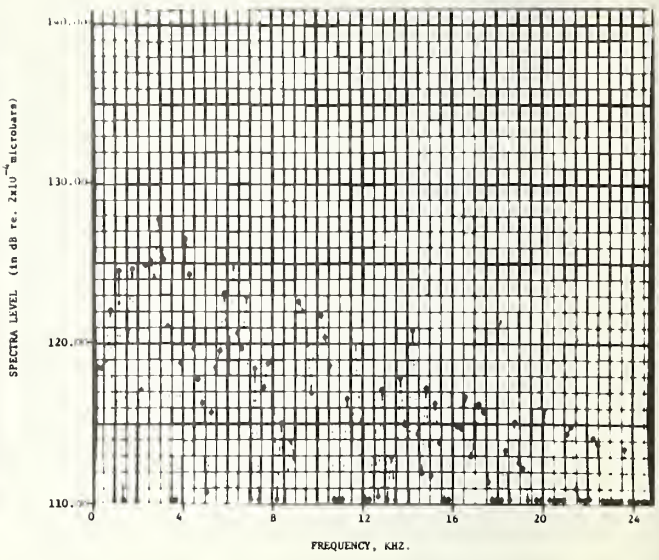

30 inches from centerline, 27 inches downstream

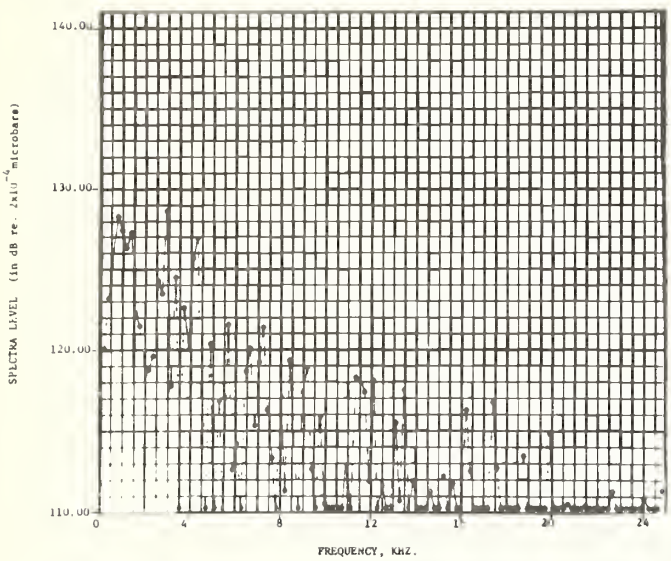

36 inches from centerline, 45 inches downstream

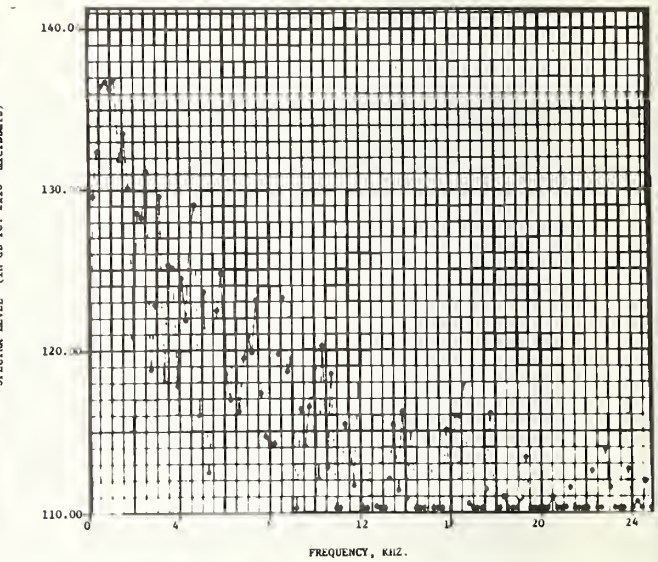

30 inches from centerline, 54 inches downstream

FREQUENCY SHIFT OBSERVED FROM THE B&K MICROPHONE POSITIONS ALONG THE 144 dB CONTOUR OF THE OVEREXPANDED JET.

Figure 11

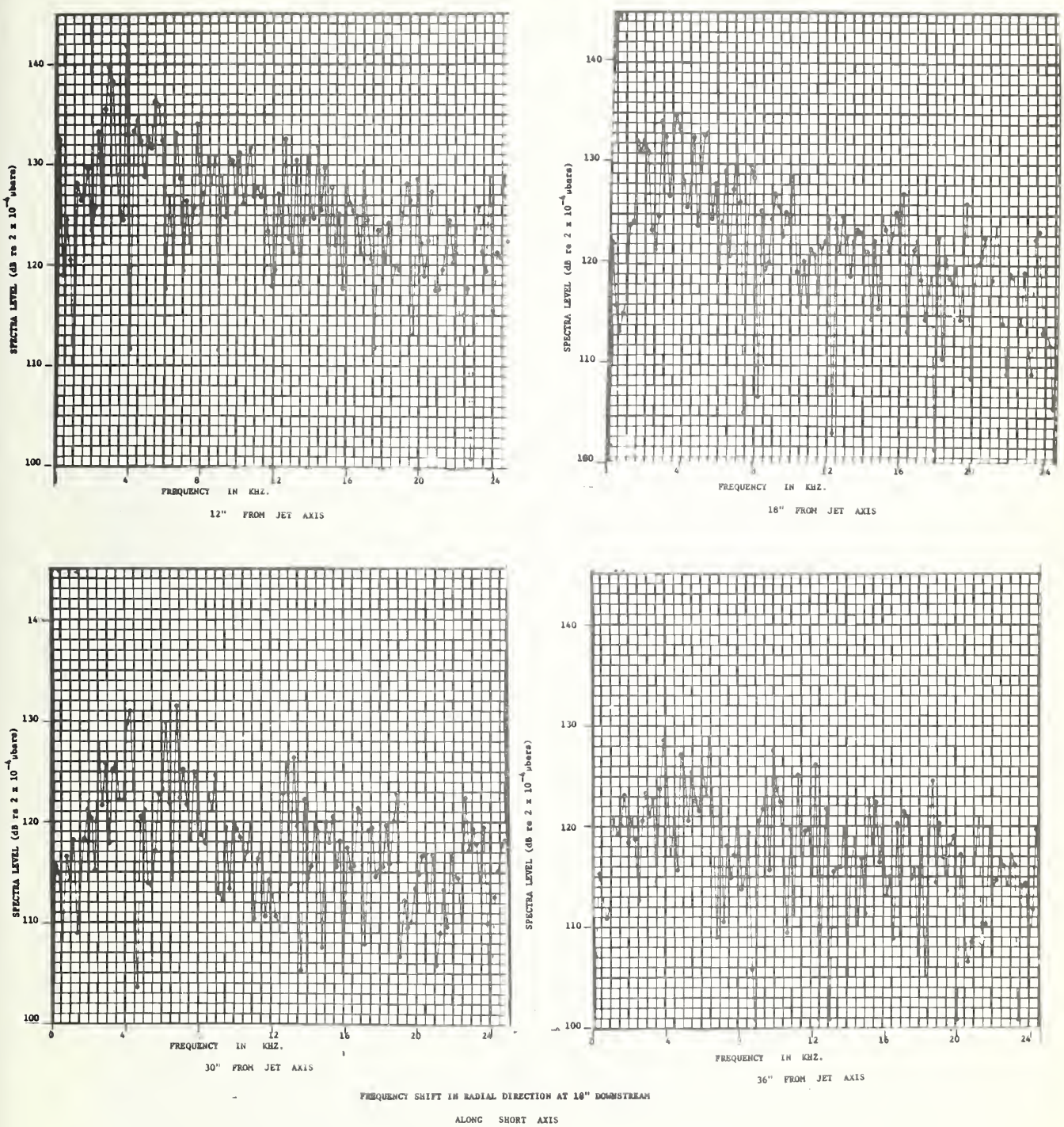

Figure 12: Frequency shift in a traverse direction to the jet axis (overexpanded rectangular jet)

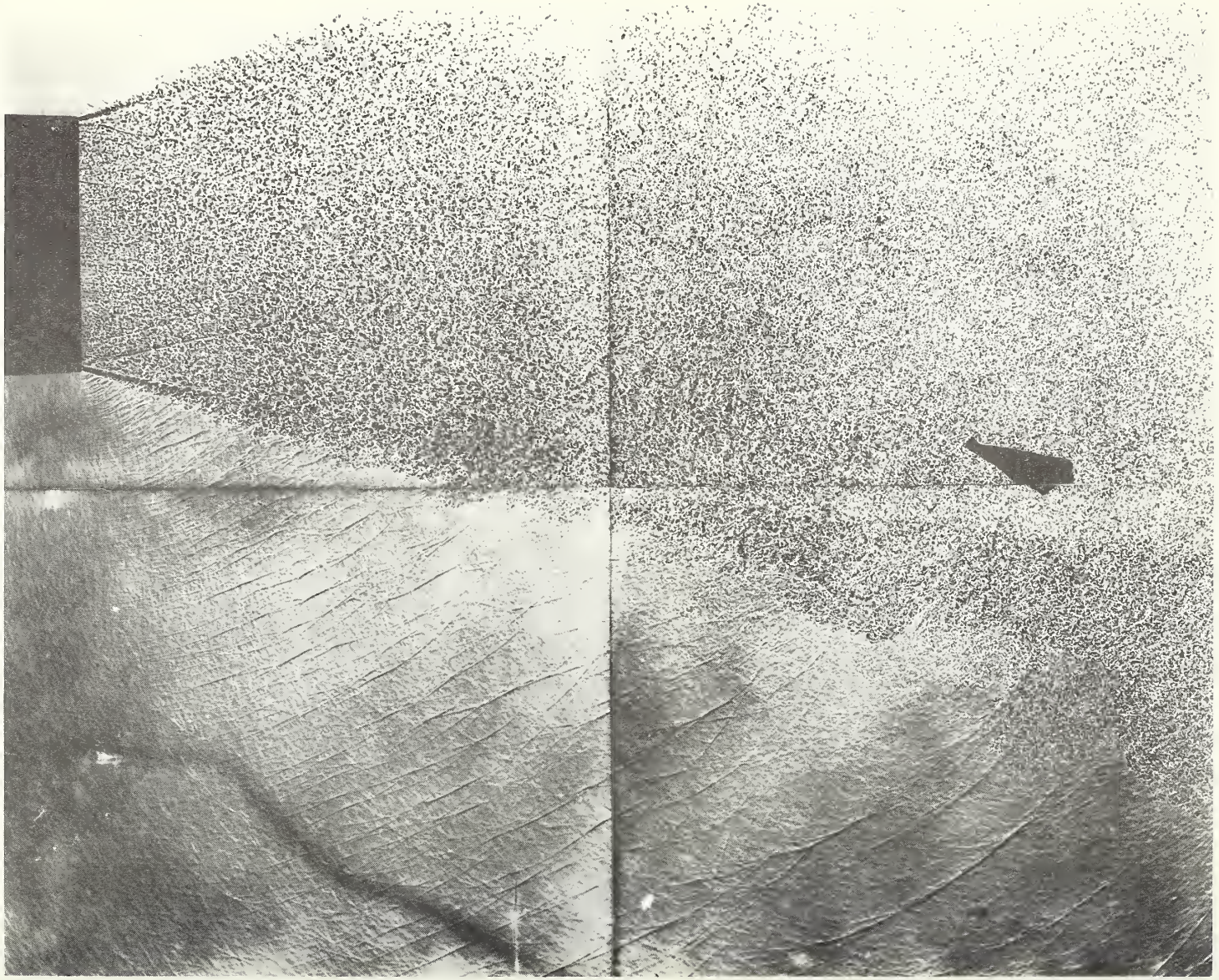

Figure 13: Underexpanded rectangular jet shadowgraph along the long axis

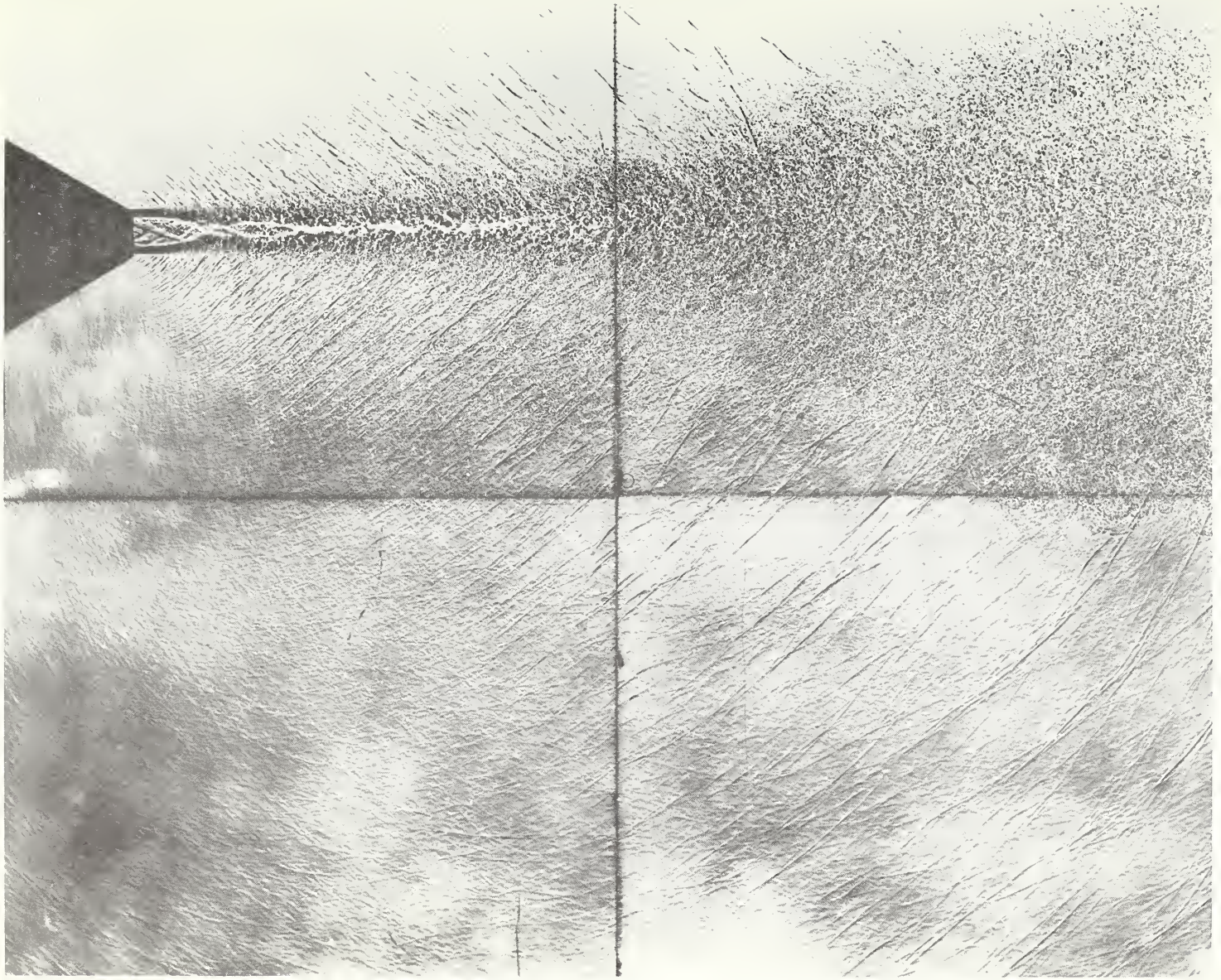

Figure 14: Perfectly expanded jet shadowgraph along the short axis

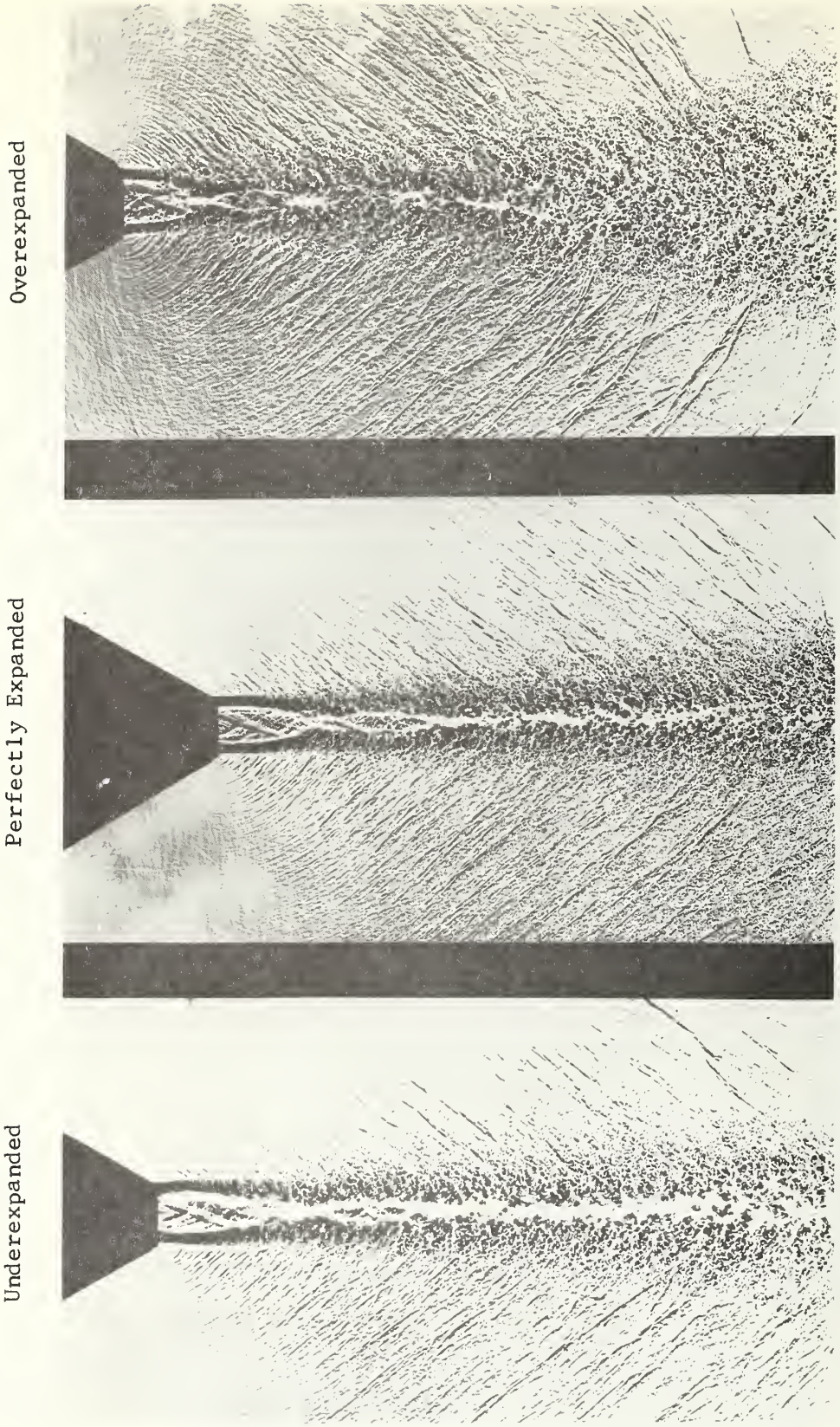

Figure 15: Shadowgraph picture for the three expansion levels (rectangular jet)

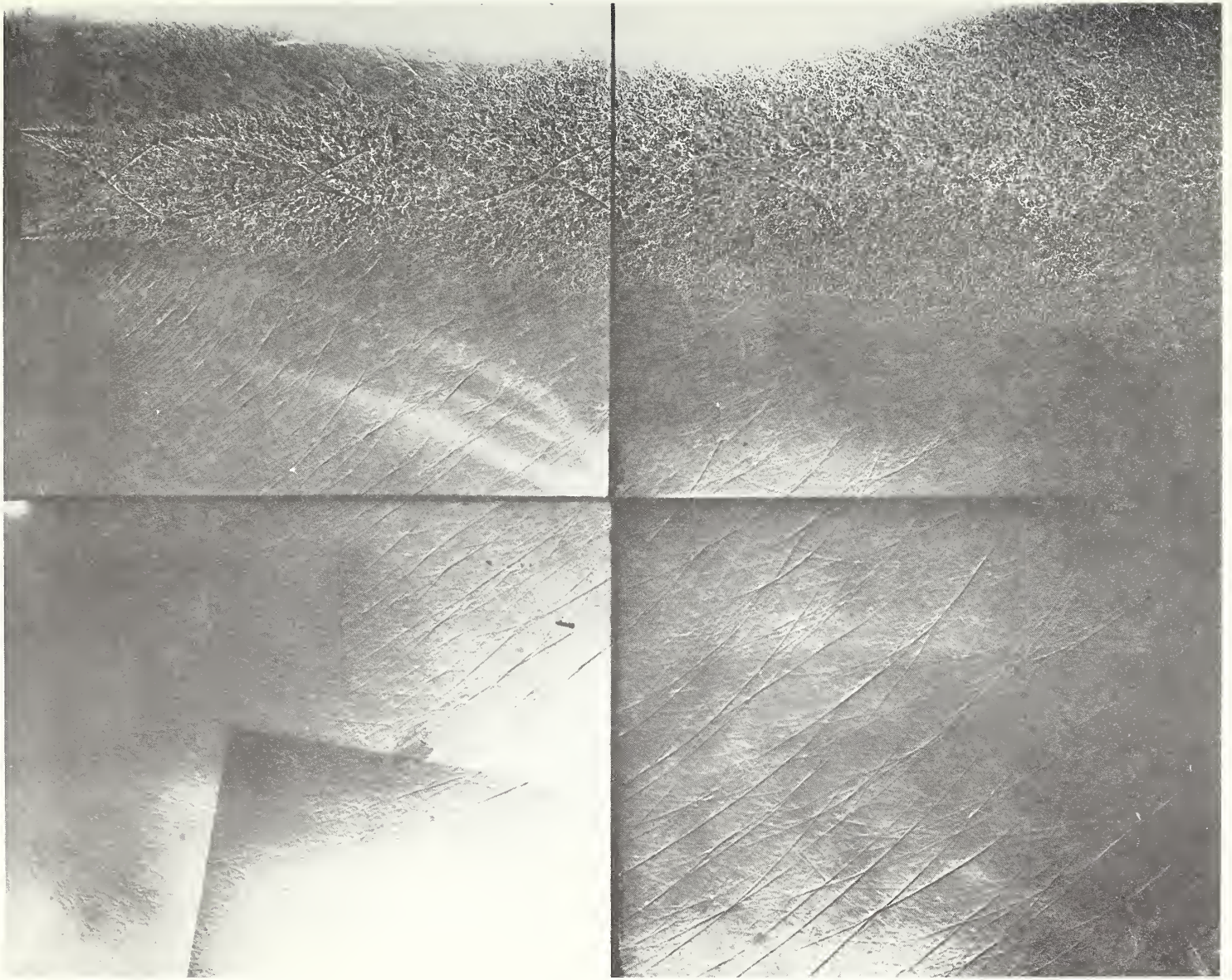

Figure 16: Shadowgraph of the overexpanded low temperature (1350° R) circular jet

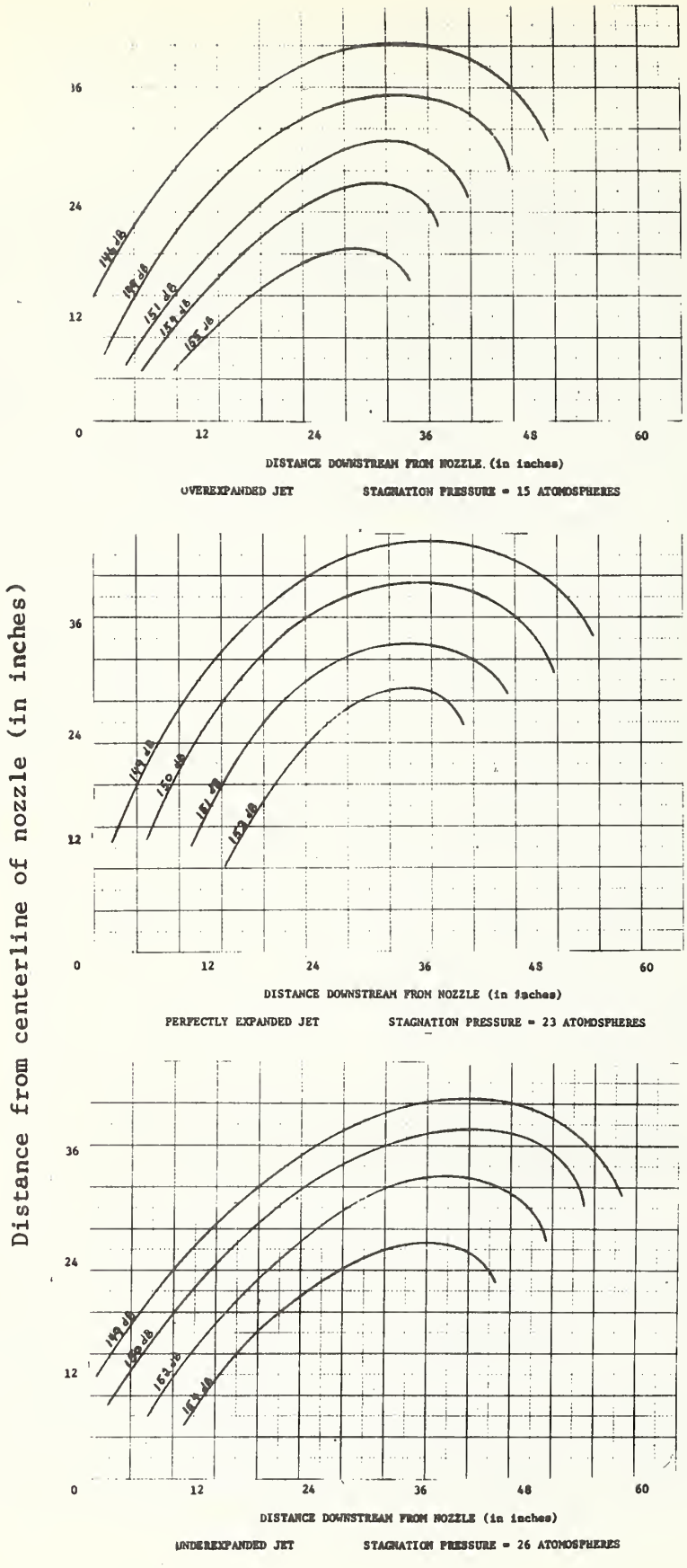
Distance from centerline of nozzle (in inches)
0
12
24
36
48
60
DISTANCE DOWNSTREAM FROM NOZZLE. (in inches)
OVEREXPANDED JET STAGNATION PRESSURE = 15 ATOMOSPHERES
DISTANCE DOWNSTREAM FROM NOZZLE (in inches)
PERFECTLY EXPANDED JET STAGNATION PRESSURE = 23 ATOMOSPHERES
DISTANCE DOWNSTREAM FROM NOZZLE (in inches)
UNDEREXPANDED JET STAGNATION PRESSURE = 26 ATOMOSPHERES

Figure 17: Directivity pattern of the high stagnation temperature circular jet (4900° R)

Figure 18

Ellipticity as a Function of Axial Distance on a Cylindrical Surface of Radius 36" Coaxial to Jet

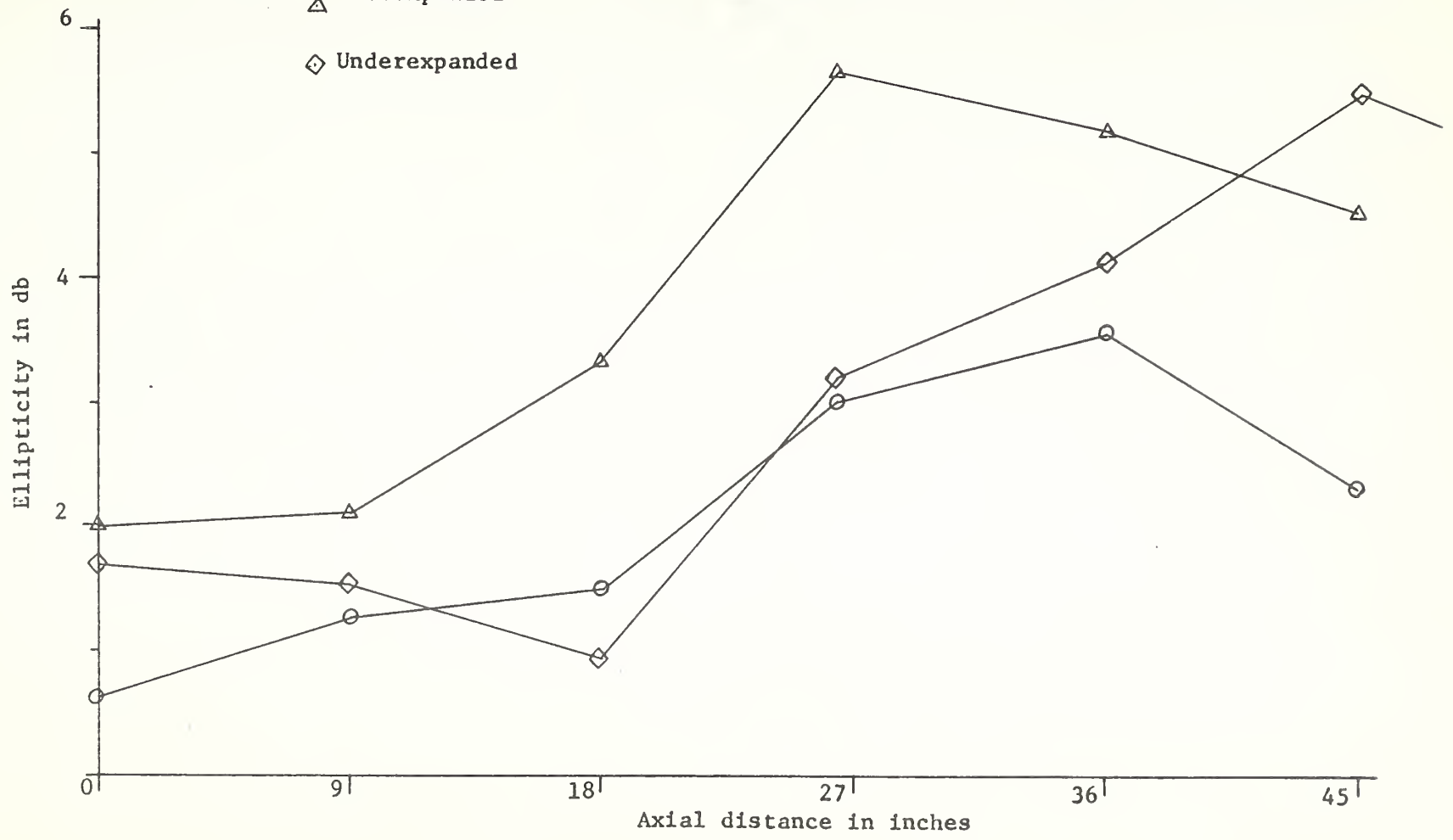

Figure 19

AXIAL DISTRIBUTION OF INTENSITY
AT DISCRETE FREQUENCIES

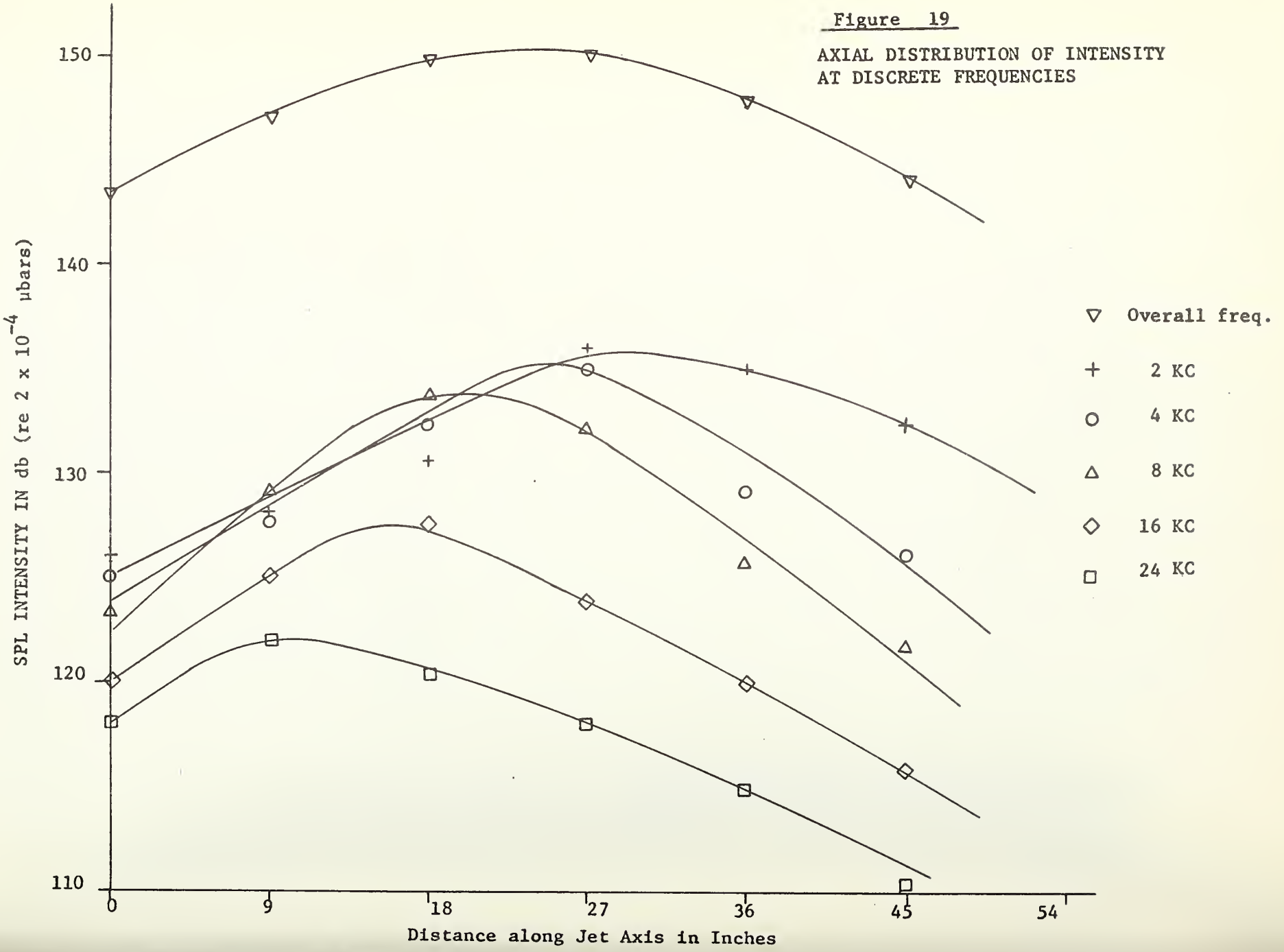

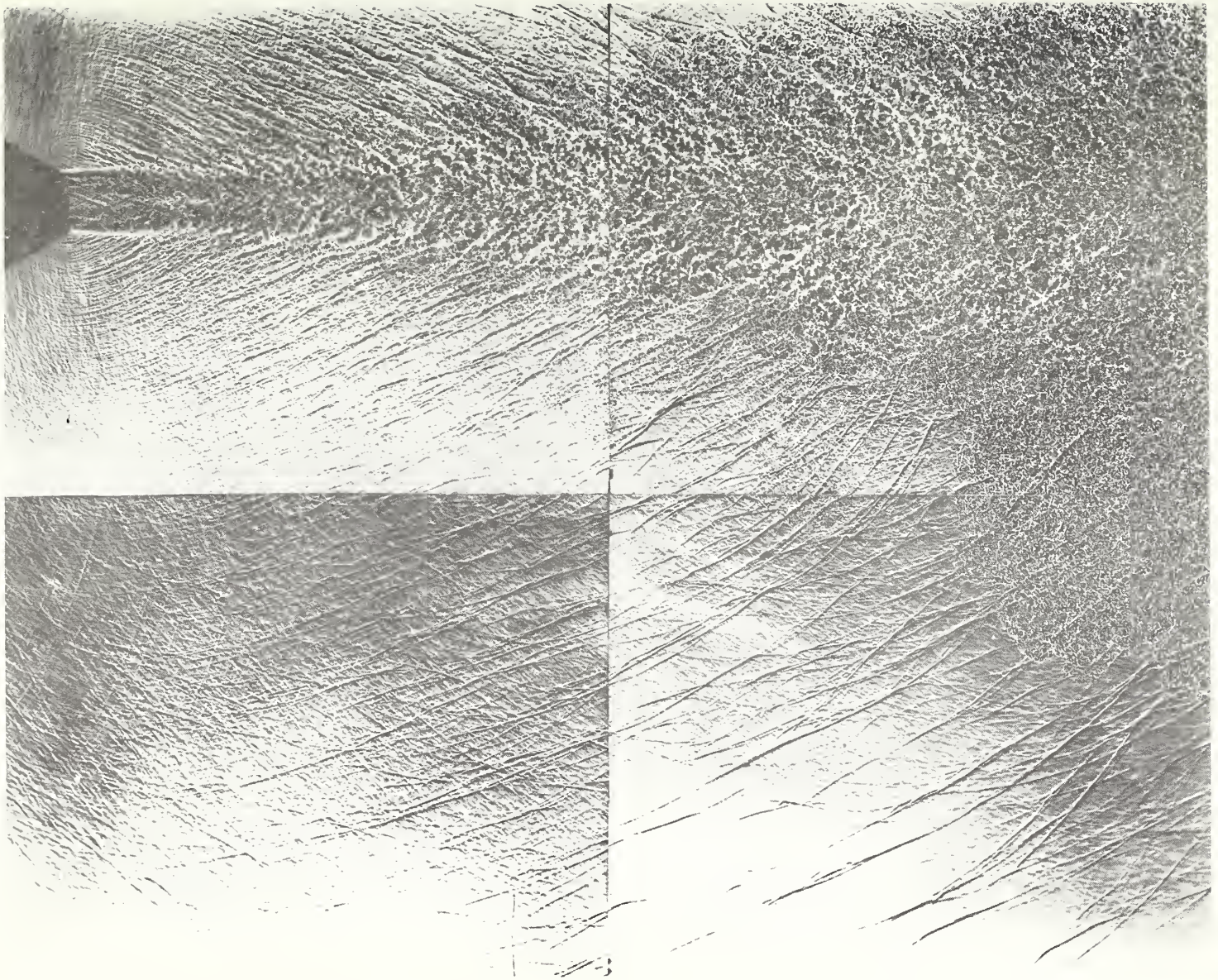

Figure 20: High temperature (4900°R) perfectly expanded rectangular jet shadowgraph

Figure 21: Shadowgraph for high temperature (4900°R) overexpanded circular jet

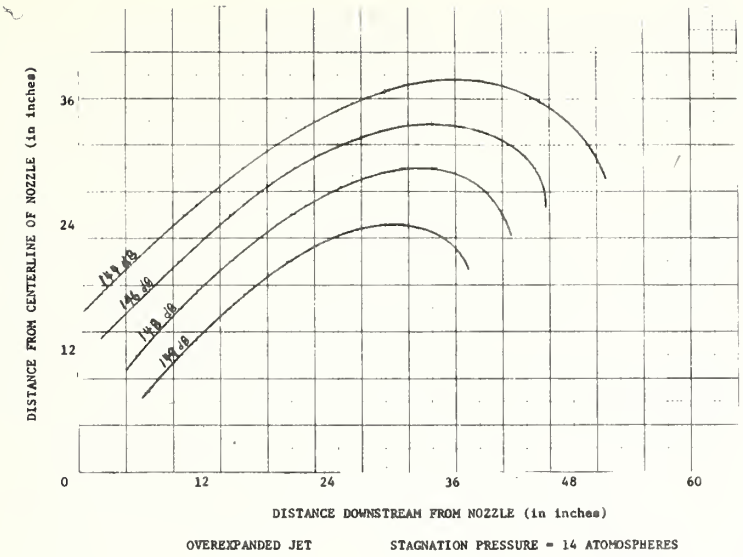

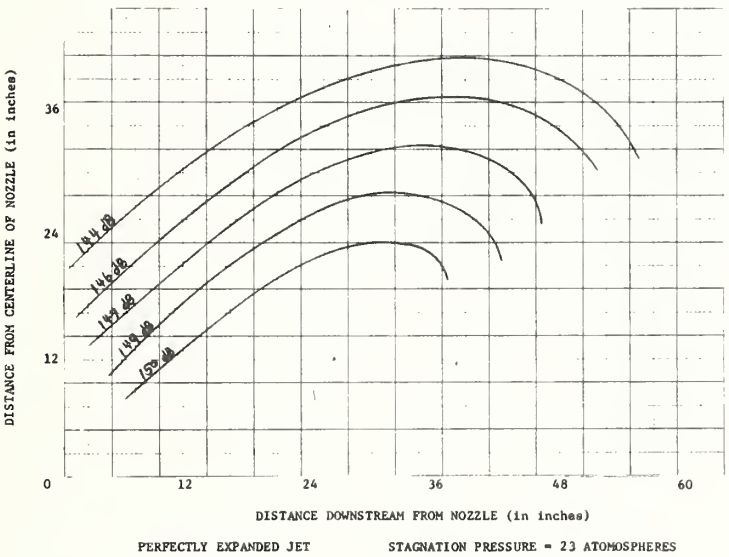

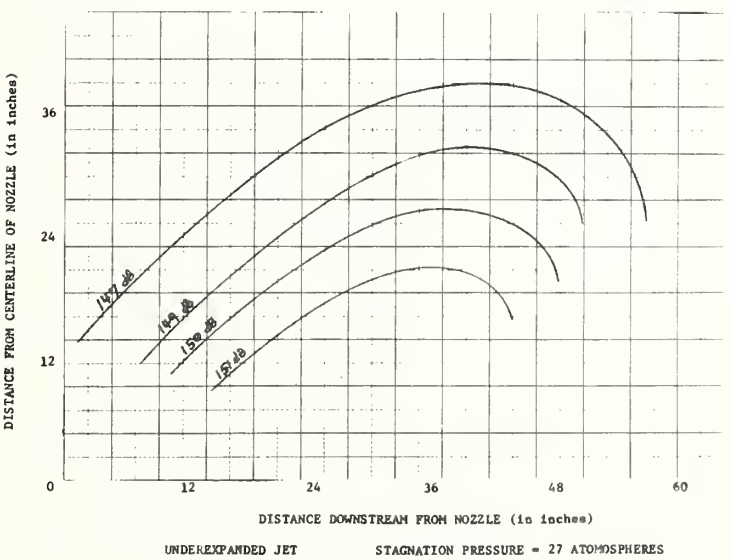

Figure 22: Directivity patterns of the contours of constant db levels for a stagnation temperature of 2900°R (circular jet)

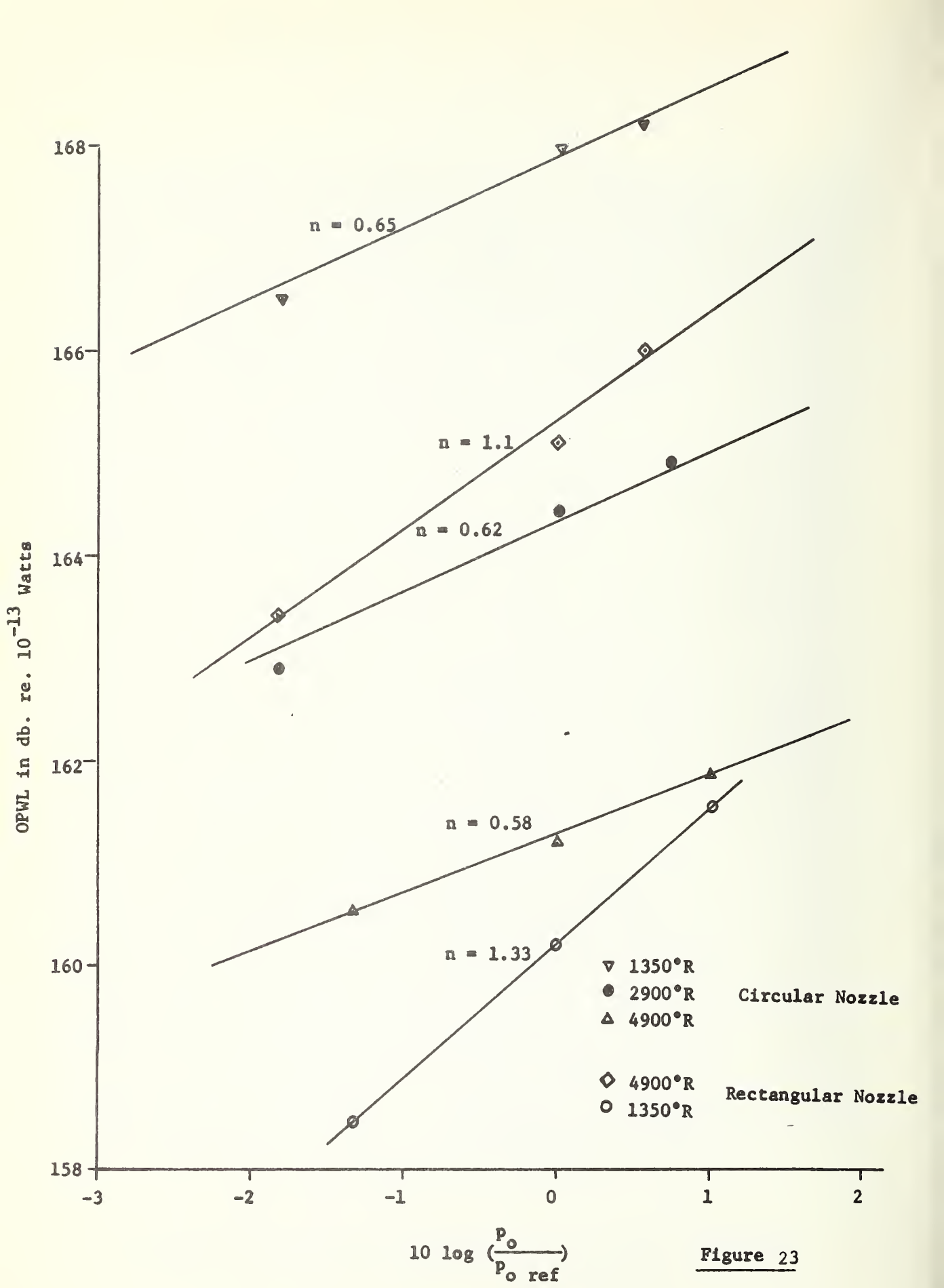
168
166
164
162
160
158
-3
-2
-1
0
1
2
OPWL in db. re. 10^{-13} Watts
10 log ($\frac{P_o}{P_{o\ ref}}$)
n = 0.65
n = 1.1
n = 0.62
n = 0.58
n = 1.33
1350°R
2900°R
4900°R
Circular Nozzle
4900°R
1350°R
Rectangular Nozzle

Figure 23

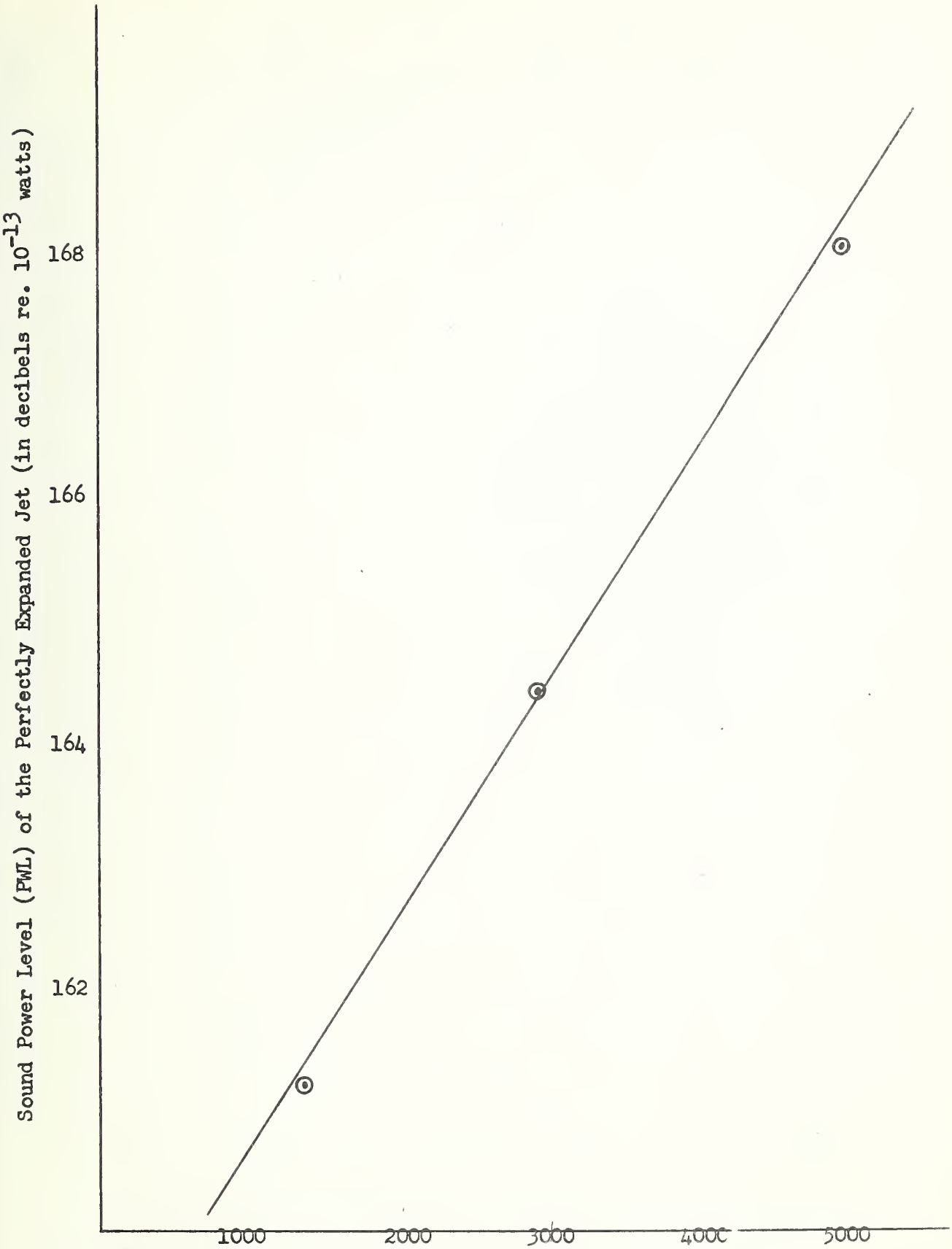
Sound Power Level (PWL) of the Perfectly Expanded Jet (in decibels re. 10^{-13} watts)
168
166
164
162
1000
2000
3000
4000
5000
Stagnation Temperature
(in degrees Rankine)

FIGURE 24

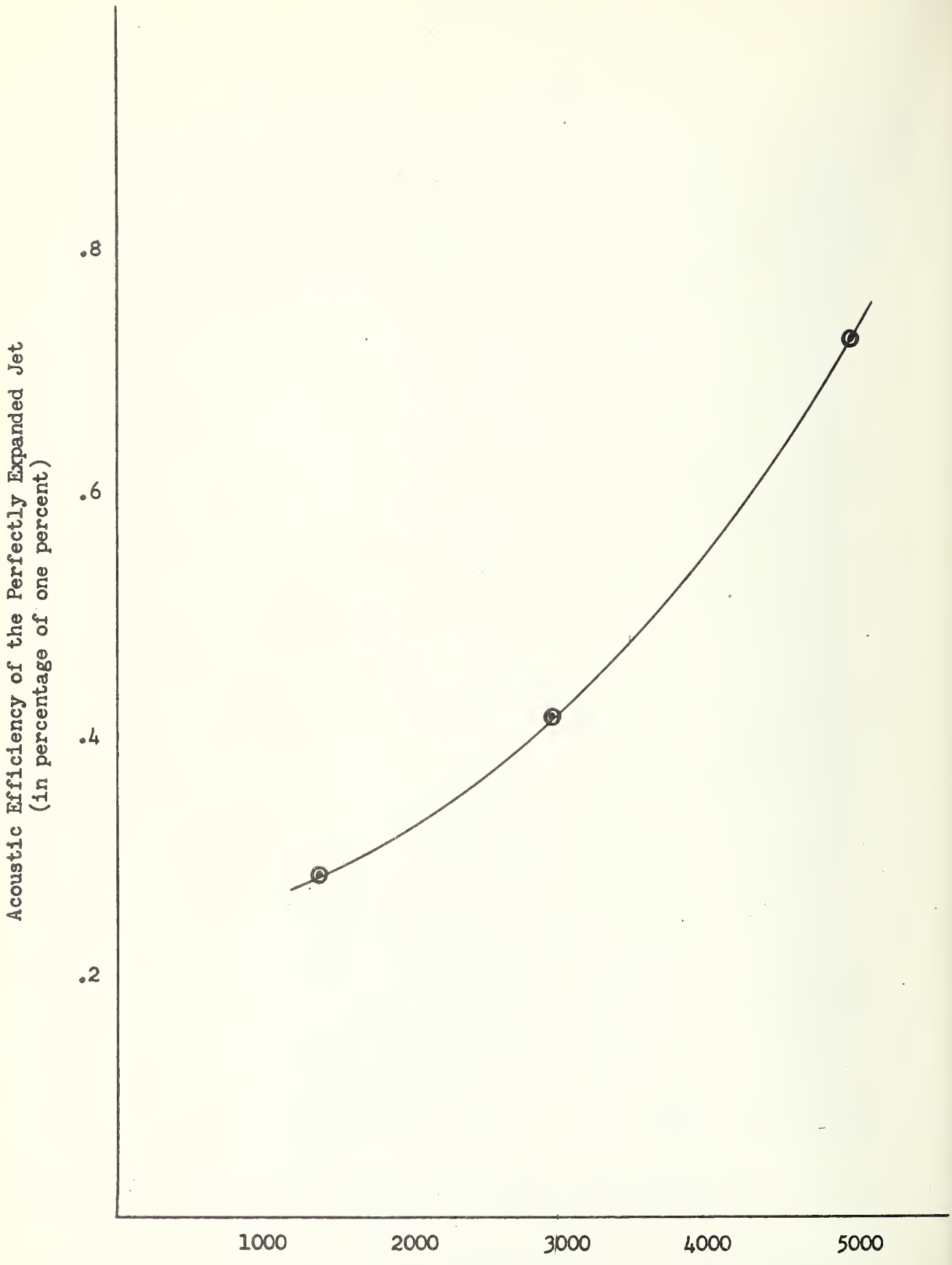
Acoustic Efficiency of the Perfectly Expanded Jet
(in percentage of one percent)
.8
.6
.4
.2
1000
2000
3000
4000
5000
Stagnation Temperature
(in degrees Rankine)

FIGURE 25

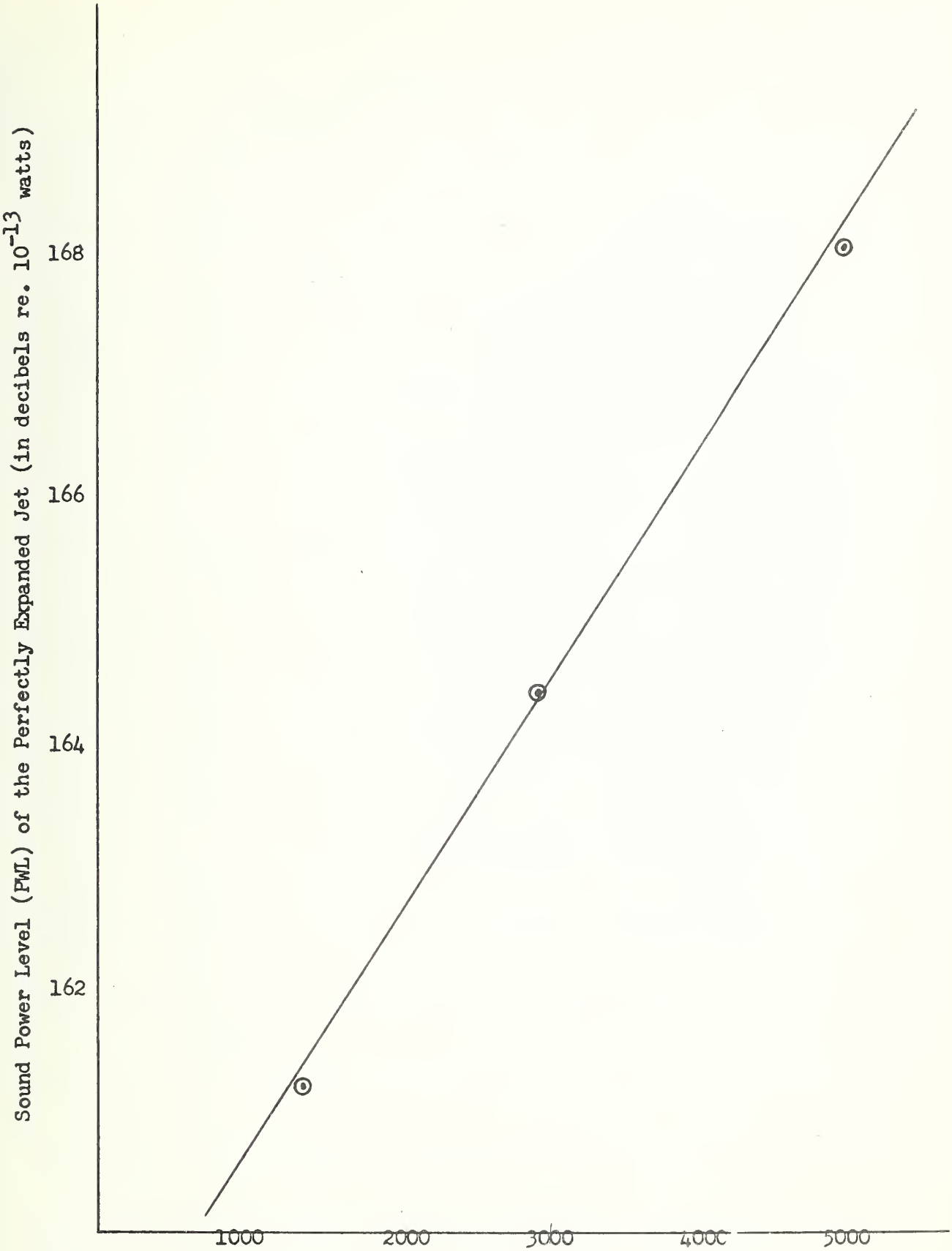
Sound Power Level (PWL) of the Perfectly Expanded Jet (in decibels re. 10^{-13} watts)
168
166
164
162
1000
2000
3000
4000
5000
Stagnation Temperature
(in degrees Rankine)

FIGURE 24

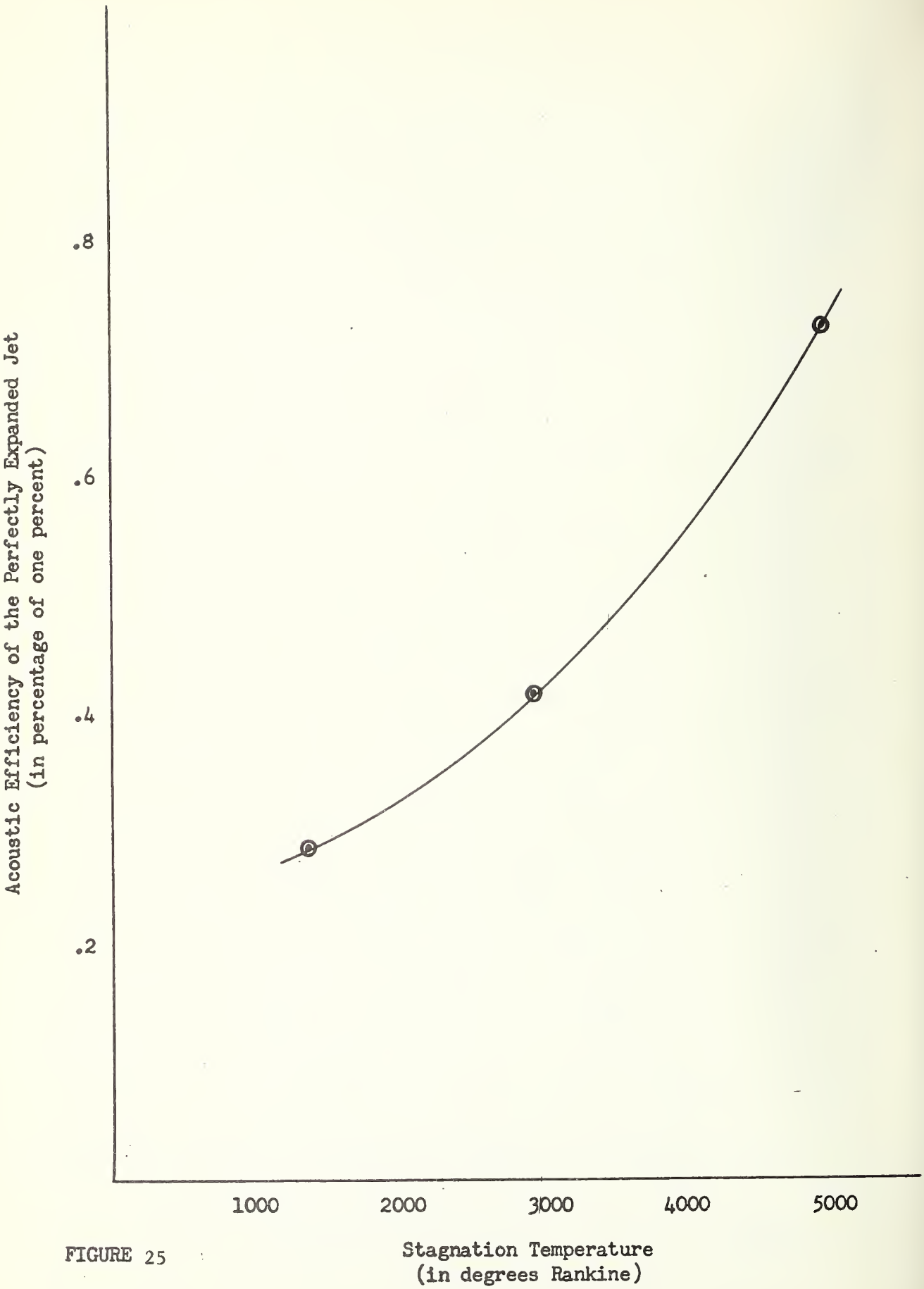
Acoustic Efficiency of the Perfectly Expanded Jet
(in percentage of one percent)
.8
.6
.4
.2
1000
2000
3000
4000
5000
Stagnation Temperature
(in degrees Rankine)

FIGURE 25

REFERENCES

1. Lighthill, M. J., "On Sound Generated Aerodynamically: I. General Theory," Proceedings of Roy. Soc., Ser. A, Vol. 211, 1952.

   __, "On Sound Generated Aerodynamically: II. Turbulence as a Source of Sound," Proc. of Roy. Soc., Ser. A, Vol. 222, 1954.

2. Tam, C.K.W., "Directional Acoustic Radiation from a Supersonic Jet Generated by Shear Layer Instability," J. of Fluid Mech., 46, 757, 1971.

3. Ffowcs Williams, J. E., "Noise from Turbulance Convected at High Speed," Phil. Trans. Roy. Soc., A255, 1963, pp. 469-503.

4. Lin, J.T.C., "On Eddy Mach Wave Radiation Source Mechanism in the Jet Noise Problem," AIAA, 71-150.

5. Ribner, H. S., "Eddy Mach Wave Noise from a Simplified Model of a Supersonic Mixing Layer," NASA SP 207, p. 53.

6. Nagamatsu and Horvay, "Supersonic Jet Noise," AIAA, 70-237.

7. Potter, R. C., "An Investigation to Locate the Acoustic Source in a High Speed Jet Exhaust Stream," Wyle Labs, TR WR 68-4.

8. Nagamatsu, Sheer and Gill, "Flow and Acoustic Characteristics of 191 Tubes and 191 Shrouds Supersonic Jet Noise Suppressor," AIAA, 71-153.

9. Tyler, Sofrin and Davis, "Rectangular Nozzles for Jet Noise Suppression," for presentation at the SAE National Aeronautical Meeting, N.Y., March 31, 1959.

10. Coles, W. D., "Jet Engine Exhaust Noise from Slot Nozzles," NASA TND 60, 1959.

11. Simcox, C. D., "Effect of Temperature and Shock Structure on Choked Jet Noise Characteristics," AIAA, 71-582.

12. Letty, R., Study of Jet Noise from a Supersonic Axisymmetric Nozzle, S.M. Thesis, Aero and Astro Dept., M.I.T., 1971.

13. Zaic, G. F., Holographic Visualisation of Sound Generated by a Supersonic Jet Impinging on a Wedge, S.M. Thesis, M.E. Dept., M.I.T., 1971.

14. Kolesar, R. R., Optical Holographic Investigation of the Acoustic Field Associated with a Cold Supersonic Jet, S.M. Thesis, M.E. Dept., M.I.T., 1971.

15. Gaydan, A. G., Shock Tube in High Temperature Chemical Physics, Reinhold Pub. Corp., N.Y., 1963.

16. Lin, S. C., "Production of High Temperature Gases in Shock Tubes," J. of App. Physics, Vol 23, 12, 1952.

17. Kornberg, J. P., Study of Jet Noise from a Supersonic Slotted Nozzle, S.M. Thesis, Aero and Astro Dept., M.I.T., 1970.

18. Voce, J. D., and Lush, P. A., An Application of Quadrupole Theory to Correlate the Directivity and Spectra of High Speed Jet Noise, Rolls Royse Ltd.

19. Jones, I.S.F., "Finite Amplitude Waves from a Supersonic Jet," AIAA 71.151.

20. Lasseter and Hubbard, "Experimental Studies of Noise from Subsonic Jets in Still Air," NACA TN 2757.

21. Plumblee, H. E., "Effect of Duct Heating on Jet and Fan Noise," NASA SP 207, p. 113.

22. Christensen, E. M., "Jet Noise and Shear Flow Instability seen from an Experimenter's Viewpoint," J.of Appl. Mech., Vol. 34, March 1967.

23. Patel, Jayanti, "Jet Noise from a Supersonic Rectangular Nozzle," S.M. Thesis, Aero. and Astro. Dept., MIT, Sept. 1971.

HE 18.5
.A38 no.
DOT-TSC-
142-1

BORROWER

Form DOT F 1720.2
FORMERLY FORM DOT F

DOT LIBRARY
00351845